[UCI]I804:48009-200000284779

Master Thesis

Harvesting Energy from Fluid-based Triboelectric Nanogenerator and its Versatile Applications as Mechanical Transducer

University of Ulsan

School of Mechanical Engineering

M. SHAHRIAR

February 2020

유체 기반 Triboelectric Nanogenerator 를 통한

에너지 수확 및 기계식 Transducers 로의 다양한 응용

Harvesting Energy from Fluid-based Triboelectric Nanogenerator and its Versatile Applications as Mechanical Transducer

지도교수 안경관

이논문을 공학석사 학위 논문으로 제출함

2020 년 02 월

울산대학교 대학원

울산대학교 기계공학부

M. Shahriar

Harvesting Energy from Fluid-based Triboelectric Nanogenerator and its Versatile Applications as Mechanical Transducer

Supervisor: **Prof. Kyoung Kwan Ahn**

A Thesis Submitted to the School of Mechanical Engineering and the Graduate School of university of Ulsan, Republic of Korea in partial fulfillment of the requirements for *the degree of Master of Science in Mechanical Engineering*

By

M. SHAHRIAR

February 2020

This certifies that the thesis of

M. SHAHRIAR is approved

Thesis committee Chairman	**Professor Yang Soon young**
Thesis committee Member	**Professor Lee Byung Ryong**
Thesis committee Member	**Professor Ahn Kyoung Kwan**

The Graduate School

University of Ulsan

February 2020

M SHAHRIAR 의

공학석사 학위 논문을 인준함

심사위원	**양순용**	인
심사위원	**이병룡**	인
심사위원	**안경관**	인

울 산 대 학 교 대 학 원

기계자동차공학과

2020 년 02 월

ACKNOWLEDGEMENTS

Firstly, I am very thankful to almighty ALLAH for his blessings upon me in my whole life.

I would like to express my deepest gratitude to my advisor, Professor Ahn, Kyoung Kwan, for his great support, guidance and providing me with an excellent atmosphere for doing research. Being almost a novice in experimental research, his constant support has led me to learn how to accomplish the experiment and analyze the results properly. It is a great understatement to say that this work would not have been completed without his help. I express the special gratitude to him for the excellent effort and patience on me to train me up.

My sincere thanks to my Flu-TENG project mates in Fluid Power and Machine Intelligence Lab, specially Vo Cong Phat, Le Chau Duy, Ravi Kumar Cheederela who supported me lot during my learning phase and to prepare for the review answers for the accepted journals. The outstanding friendly nature inside the laboratory helps me incredibly to do research.

Finally, I would like to thank and express my gratitude towards my parents without whom I cannot come long way at the current situation. Their endless sacrifice has endowed me with certain bright future. At the end I would like to thank to all of my friends, previous supervisors and well wishers whose inspiration and prayers are always with me.

Best regards

M. Shahriar

November 2019, Ulsan, South Korea

ABSTRACT

With the increasing demand of electricity supply and usage of portable electronics in our day to day life, self-powered system has brought a revolutionary change in the recent decades to mitigate the excess pressure on power grid. Following the other nanogenerators like piezoelectric, thermoelectric, triboelectric nanogenerator (TENG) has come up with the utilization of waste mechanical energy into useful power sources. The main advantages of TENG over traditional battery systems are that it doesn't need to be replaced over time, can continuously harvest energy from the ambient source that can be stored in the capacitors for future supply, very flexible.

Triboelectric nanogenerator (TENG) comprises of the contact electrification and electrostatic induction. When two dissimilar materials are bought into physical contact with each other due to electrostatic induction there is a redistribution of charges with the opposite sign on the two surfaces according to tribopolarities. After a while, separation occurs by means of any external mechanical force which induces triboelectricity that can generate a potential drop and drive the electrons to flow between the electrodes attached with the surfaces. TENG has four fundamental modes till now, including, vertical contact-separation mode, lateral sliding mode, singe electrode mode, freestanding sliding mode. In addition, a lot of structures, prototypes and functions have already been reported and are still going on.

Mostly triboelectric devices involve solid-solid contact electrification. The charge generation through friction process solely depends on the difference of the ability of the two surfaces to loss or gain electrons. Electrical output can be improved via change of the surface morphological properties in this process. Nevertheless, the performance can be greatly influenced by the air humidity, dust, which causes instability of the output values of the solid-solid TENG without any encapsulation.

Also wear abrasion due to physical collision deteriorates the long-term output stability of the TENG. However, liquid-solid contact electrification has demonstrated the capability of stable response with full contact separation process with the counter solid part. The output shows regular behavior for long term application with good wear resistance while using the liquid for contact. In liquid-solid TENG, the liquid can change its shape and mostly work as a positive tribo-material that exhibit feasibility to be used in flexible and wearable sensor applications. Considering possible advantages of the liquid in TENG application, in this thesis, I've taken in account the fluid-structure interaction problem for two cases peristaltic flow in elastic tubing as energy harvester and velocity sensor on the other hand, PDMS based microfluidic platform to sense the pressure and frequencies of the rotary actuator that manipulates the motion discrete liquid column in the channel over thin polymeric film. In the first investigation, a relationship has been developed between the peristaltic laminar flow dynamics while interacting with the PVDF microporous membrane and the generation of voltage and current. Moreover, the described energy harvester can also work as flow sensor. From the second investigation, it is found that, the MEMS device can be effectively used as the transducer to measure the certain frequencies and pressures of rotary actuator

TABLE OF CONTENTS

LIST OF FIGURES

CHAPTER 1

INTRODUCTION

1.1. Scavenging waste mechanical energy

Due to the scarcity of fossil fuels and its abundant use in our daily life, much attention is now given on alternative sources of energies utilizing the possible renewable sources like wind, solar and geothermal process. These sources of energy are now functioning to be coupled with large scale power grids, industrial sectors or certain localities to meet up the demand of the excess electricity supply and lessen the excess pressure on the fossil fuel use. Following this trend, harnessing energy from waste mechanical energy from the ambient environment can solve the energy crisis for powering up the portable electronics when the traditional energy sources are unreachable. For instance, recharging the batteries for a large number of mobile sensor network or portable electronics is nearly a sturdy work, harvesting energy from the ambient environment and store the energy will ensure the continuous supply of power for better and extended lifetime. Utilizing waste mechanical energies to run the electronic devices has drawn much attention than other energy sources [1-13]. Unlike solar energy, energies from ocean wave, vibration from machineries, movement of human organs both inside and outside can be a useful source of harvest energy by deploying suitable materials with high functionality to transform the mechanical deformation or friction into supply of electrical charges. With the advent of thermoelectric, electromagnetic and piezoelectric effect-based devices, the recent decades have seen an enormous change in the field of wearable and flexible sensors with wide availability, high operability and portability [14-18]. Below, a brief discussion is delivered to have an overview on these three energy harvesting techniques.

1.1.1. Electromagnetic nanogenerator

Till now, most current generators specially AC are based on electromagnetic induction. Under the external applied mechanical force, the magnetic flux of a coil change and a current is induced in the spring or coil. This mechanism is widely used in the powerplant and has potential applications in energy harvesting purposes.

Dr. Beeby's research group [19] has developed a common example of electromagnetic nanogenerator. Four sintered magnets with high charge density were bonded manually using Cyanoacrylate to the top and bottom parts of the cantilever beam with the help of alignment jig. The magnets size was 1 x 1 x 1.5 mm^3 and 1.5 mm in the poled direction. Zinc coated mild steel keepers were used to complete the magnetic circuit and it couple the flux between top and bottom surfaces to enhance the flux gradient when the magnets start to vibrate.

While working, the generator produces a peak power of 46 μW from 60 mg acceleration across a 4000 Ω load. The power density is about 307 μWm^{-3} and the energy conversion efficiency is about 30%.

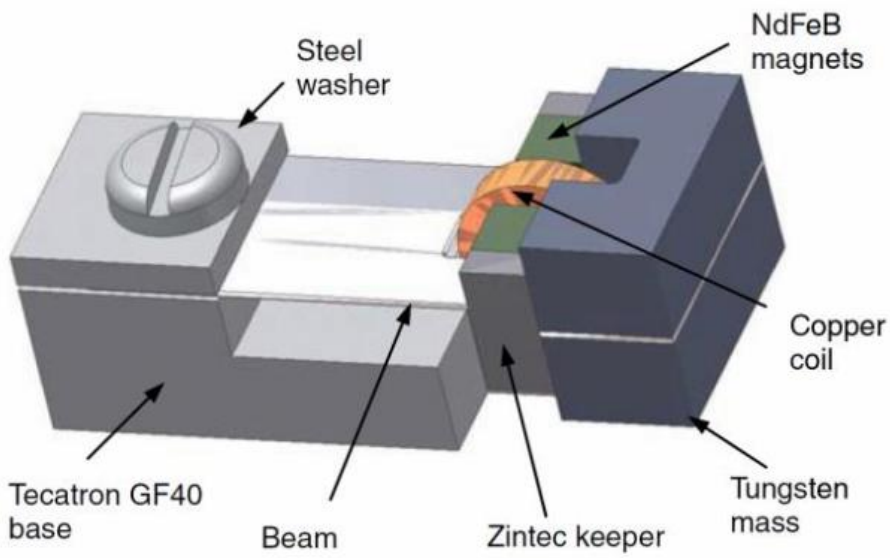

Figure 1.1 Structure of a micro-electromagnetic generator. [19]. Copyright 2007 IOP publishing.

1.1.2. Piezoelectric nanogenerator

Piezoelectric effect is extensively utilized in myriad of applications in sensors, actuators and energy harvesting [20]. Specially, the ceramic materials PVDF and PZT are the most widely used piezo materials. These materials can be differentiated with other dielectric materials by converting the applied force to the electrical signals. There are two types piezo effect one is called direct and the other converse piezoelectric effect as shown in fig.1.2. In case of direct piezoelectric effect, the applied forces change the polarizations and changes the shape in the crystal planes and this change in polarization results in the potential differences in the coated electrodes which is most favorable in the energy harvesting applications. On the contrary, under the applied electric field, the piezoelectric materials can change this shape which is called indirect or converse effect which popular in soft actuating devices [21].

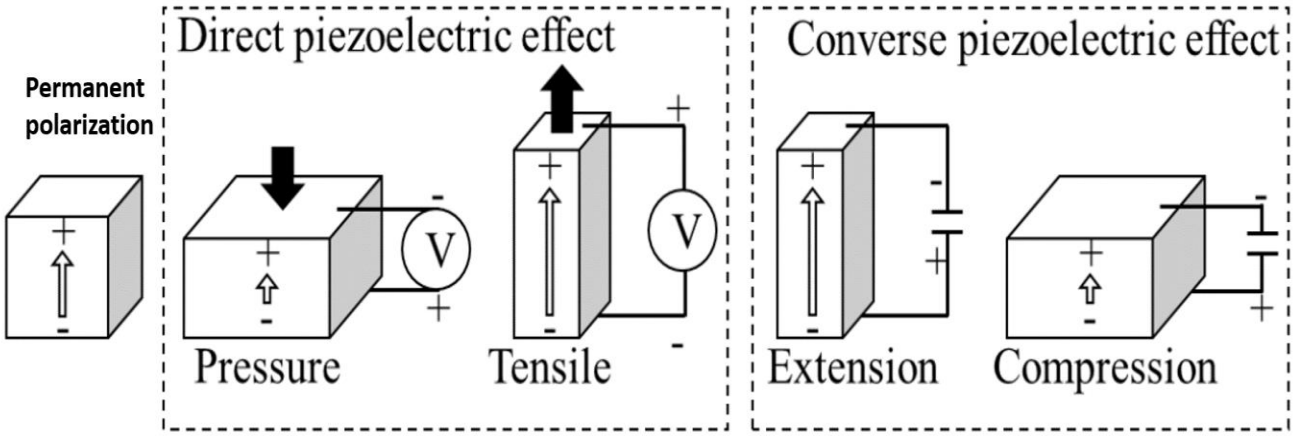

Fig. 1.2 After poling process permanent polarization happens. In direct piezo effect, applied force as pressure or tension are induced in the electrodes with the opposite polarities of the dipoles. Indirect effect is the vice versa of the direct effect.

Piezoelectric effect can be further illustrated from the report of Roundy et. Al. [22] whereas he introduced two layered members cantilever beam with both of them oppositely polarized piezo material, as shown in fig. 1.3. Under applied force bottom member suffer from compression and the top member suffer from tension. This phenomenon has generated voltage across the layers. Under the vibration and frequency of 2.5 m/s and 120 Hz respectively, it can produce an average power of 0.1 mW.

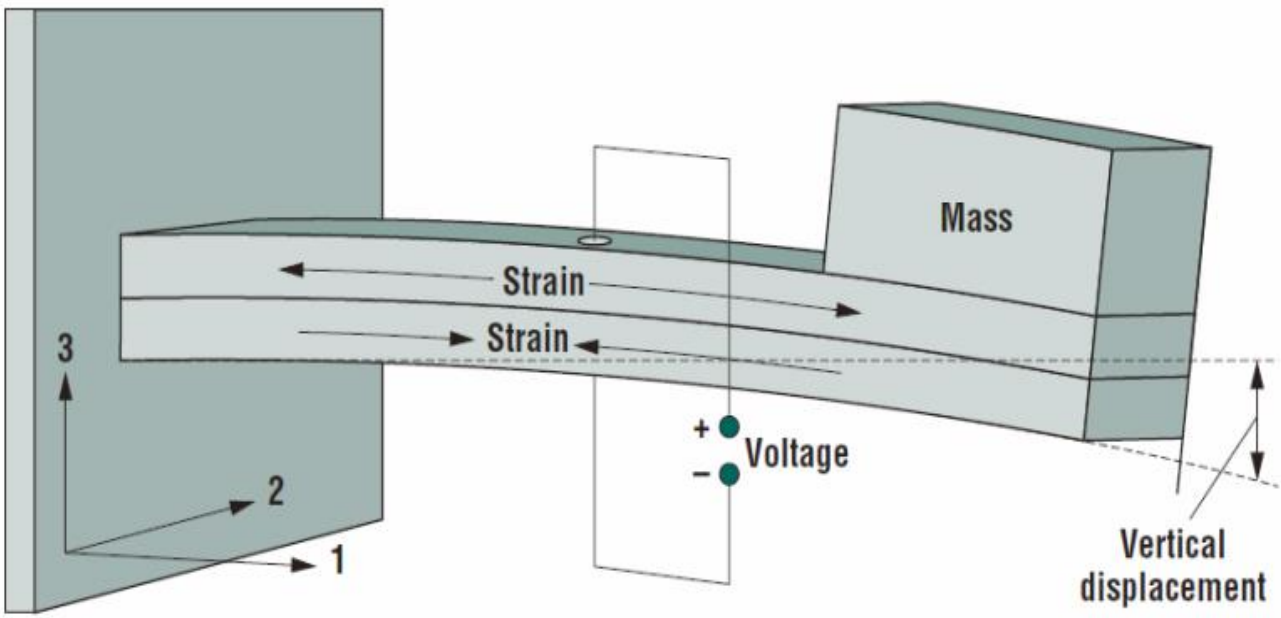

Fig.1.3. Piezoelectric nanogenerator (Roundy et.al.). A two layered cantilever with piezoelectric materials. The top layer suffers from tension and bottom layer suffers from compression under external force. (Reproduced from reference) [22]. Copyright 2005 IEEE.

One main conspicuous with the piezoelectric nanogenerator is their low output. Besides, mostly piezoelectric nanogenerator use PZT made of Lead which is toxic and has some bad environmental aspects.

1.2. Triboelectric Nano generator

Considering the demerits of the above proposed nanogenerators, in 2012 a group led by Prof. Z.L. Wang from Georgia Tech has added new dimension to the field of nanogenerators by realizing the electrical output from the friction layer of the two oppositely charged surfaces. The term is called as triboelectric nanogenerator (TENG). Till to the date, the reported TENGs has come up with certain facilities such as: Easy integration capabilities, high output power, cost effective material with low weight, simple fabrication and high efficiency. The main mechanism of TENG is a coupled effect of the contact electrification and electrostatic induction. When two dielectrics two dielectric material (or one dielectric and other one metal) has come into contact with each other due to triboelectrification and electrostatic induction. After the separation of polarized triboelectric surfaces by applied mechanical force, work is done in the external circuit to overcome the attraction force between the oppositely charged surface. Thus, mechanical energy is converted into electrical output and can be stored in capacitor and batteries for future energy demand.

CHAPTER 2

CONCEPT OF TRIBOELECTRIC NANOGENERATOR

Though the triboelectric effect has been realized long time ago, the 21st century has seen its versatile application to harvest energy as well as multiples sensors. There are speculations on the mechanism of the triboelectricity but none of them are proved yet. Though three significant phenomena can be attributed to the explanation of the triboelectrification: direct charge transfer, ion transfer and material transfer. It has the capacity to drive the charges upon the contact and sliding of dielectric materials on their surfaces. The periodic contact and separation of the dielectric surfaces causes separation in charges and induce the free charges on the coated electrodes thus generating electricity. Interestingly, not only solid materials but also pure water and liquid with different densities and metal compounds have an observable effect on the triboelectricity. Utilizing the phenomena, many water wave energy harvesting devices have been reported and have been effectively working both as harvester and salinity, concentration sensor etc [22-24].

For the TENG applications, several fundamental modes are available in terms of solid-solid and solid-liquid triboelectrification. As I've dealt with my investigation in solid-liquid TENG so the classification is discussed based on the example of solid-liquid TENG. They basic modes are:

Attached electrode 1) Contact mode TENG

2) Sliding mode TENG

Electrode arrangement 1) Single electrode mode TENG

2) freestanding triboelectric layer based nanogenerators

Below the descriptions of fundamental modes of TENGs are discussed in a nutshell.

2.1. TENG types based on friction layer

2.1.1. Contact mode TENG

A basic type of TENG is based on the vertical contact mode TENG where both solid-solid and solid-liquid arrangement is possible. Tang et.al. [25] investigated on performance of the liquid metals as an electrode with electronegative material such as PVDF, PTFE, Kapton. For this purpose, as liquid metals Galinstan and Mercury was used as shown in fig. 2.1. For the comparison various types of polymer thin film such as Kapton, PTFE, PET, PVC, PDMS, Perylene was used to measure the short circuit current and open circuit voltage and power density as shown in fig. 2.2. The proposed LM-TENG has shown high output charge density of 430 $\mu A/m^2$ which is four or five times than the solid-solid contact mode TENG. The power density subsequently obtained about 6.7 Wm^{-2} and 133 KWm^{-3}. The calculated energy conversion efficiency they obtained about 70.6%.

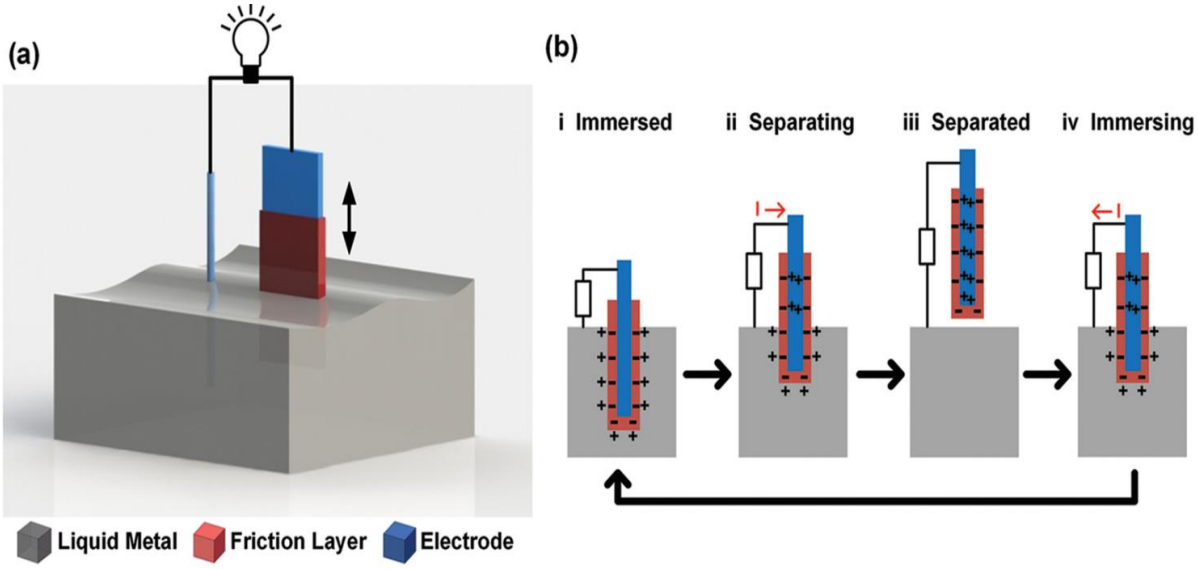

Fig 2.1 Solid-liquid contact mode TENG using the liquid metal and various electronegative material such as PTFE, PVDF, Kapton, PET etc. Reproduced from reference [25]. Copyright Adv. Funct. Materials, 2015.

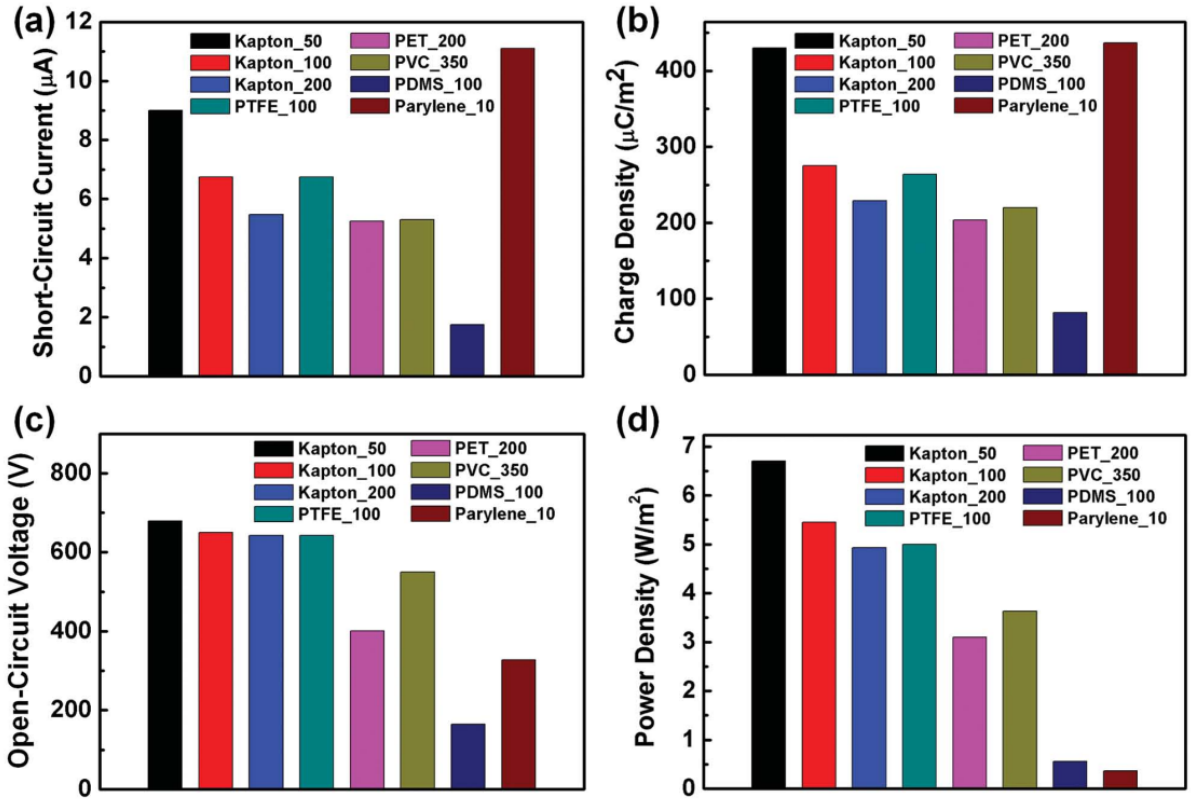

Fig 2.2. Performance analysis of LM-TENG using liquid metal and various -Ve affinity film. [25]. Copyright Adv. Funct. Materials, 2015.

2.1.2. Sliding Mode TENG

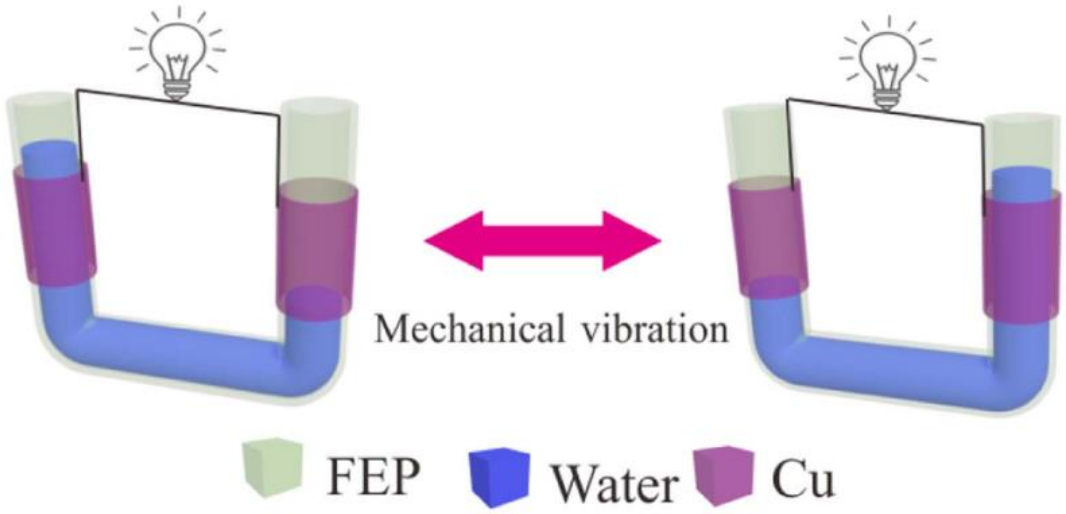

Fig 2.3. Schematic of sliding mode liquid-solid TENG using FEP & water in U-shape tubing [26]. Copyright Nano Energy 2017.

In case of sliding mode TENG, the two friction layers are come in contact together in the horizontal plane for both solid-solid and solid-liquid interface. To demonstrate this, Zhang et.al. [26] proposed a smart U-tube based TENG to be used as multifunctional sensors. For this purpose, a FEP based U-tube was used as polymer surface and Cu tape was wrapped around as shown in fig. 2.3. The water column was moving inside like slide over the electrode-FEP area under external mechanical motion. The output current and voltage can be utilized to be as sensor under external pressure difference measured by pressing the attached silicon balloon as shown in fig. 2.4

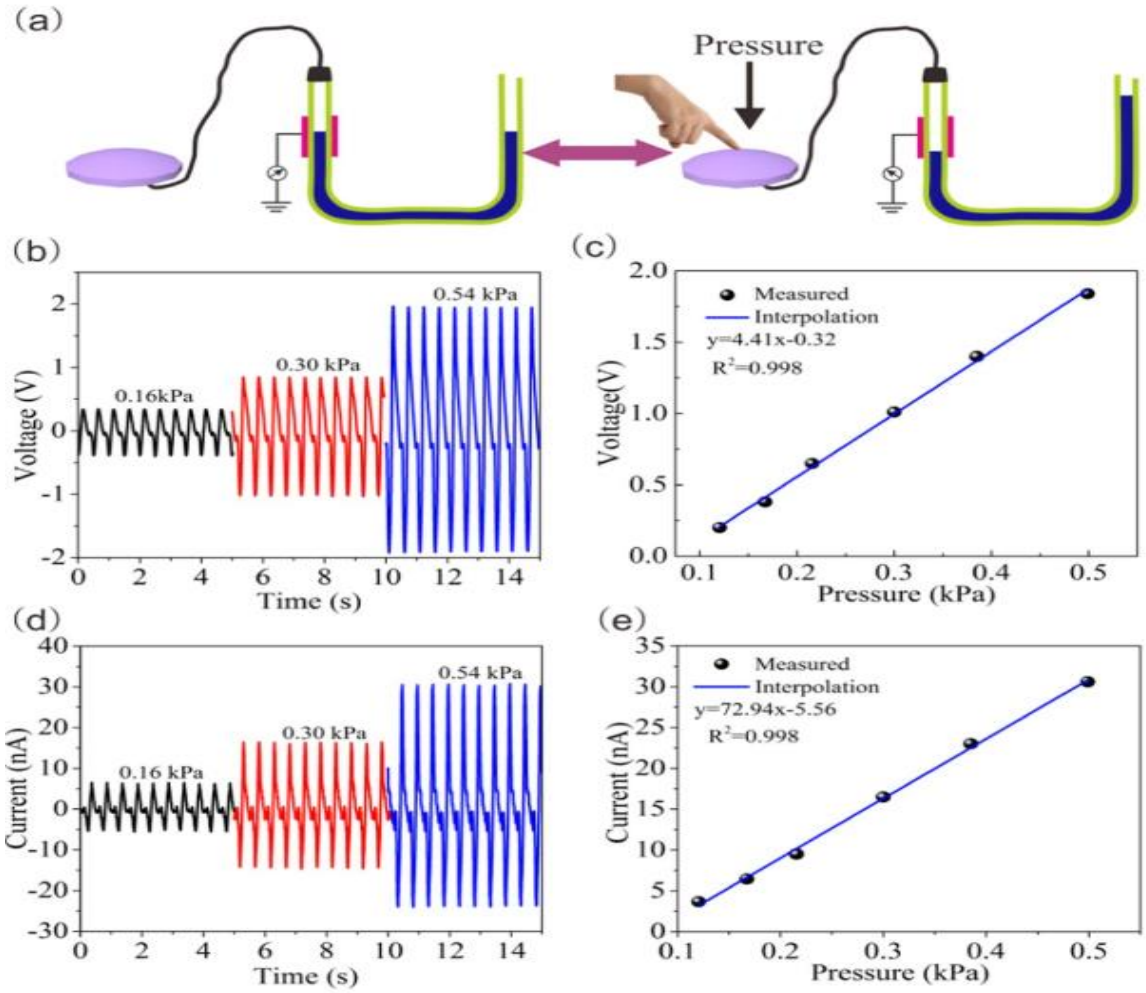

Fig. 2.4. Response of voltage and current variation U-tube TENG under different pressures (0.16 KPa, 0.30 KPa, 0.54 KPa) [26].

2.2. TENG types based on electrode arrangement

2.2.1. Single electrode mode TENG

In this type of TENG, the electrode attached with the polymer thin film becomes fixed and connected to the ground through load resistance or electrometer. A typical example can be the solid-liquid TENG to harvest water drop energy proposed by Lin et.al. [27] For this purpose, PTFE thin film was attached with the Cu electrode and then the wire from the electrode was connected to the ground through electrometer as shown in fig. 2.5.

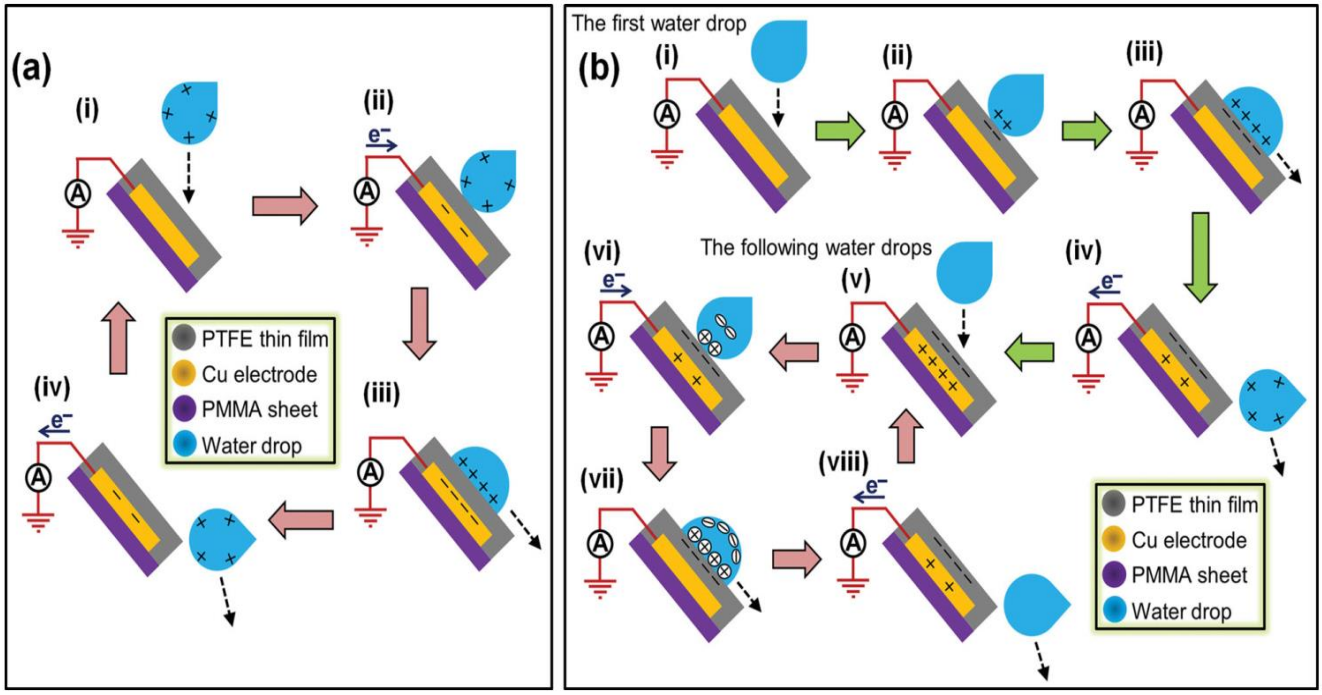

Fig. 2.5. (a) Working mechanism of the water-TENG when the generated triboelectricity is dominated by the contact electrification process with the air/pipes. (b) Working mechanism of the water-TENG when the generated triboelectricity is dominated by the contact electrification process with the PTFE thin film.

The output of the water TENG obtained from the 30 μL water droplet peak voltage 9.3 V and peak current of 17 μA. When connected to 5 MΩ load resistance the maximum output power was achieved 145 μW as shown in fig 2.6.

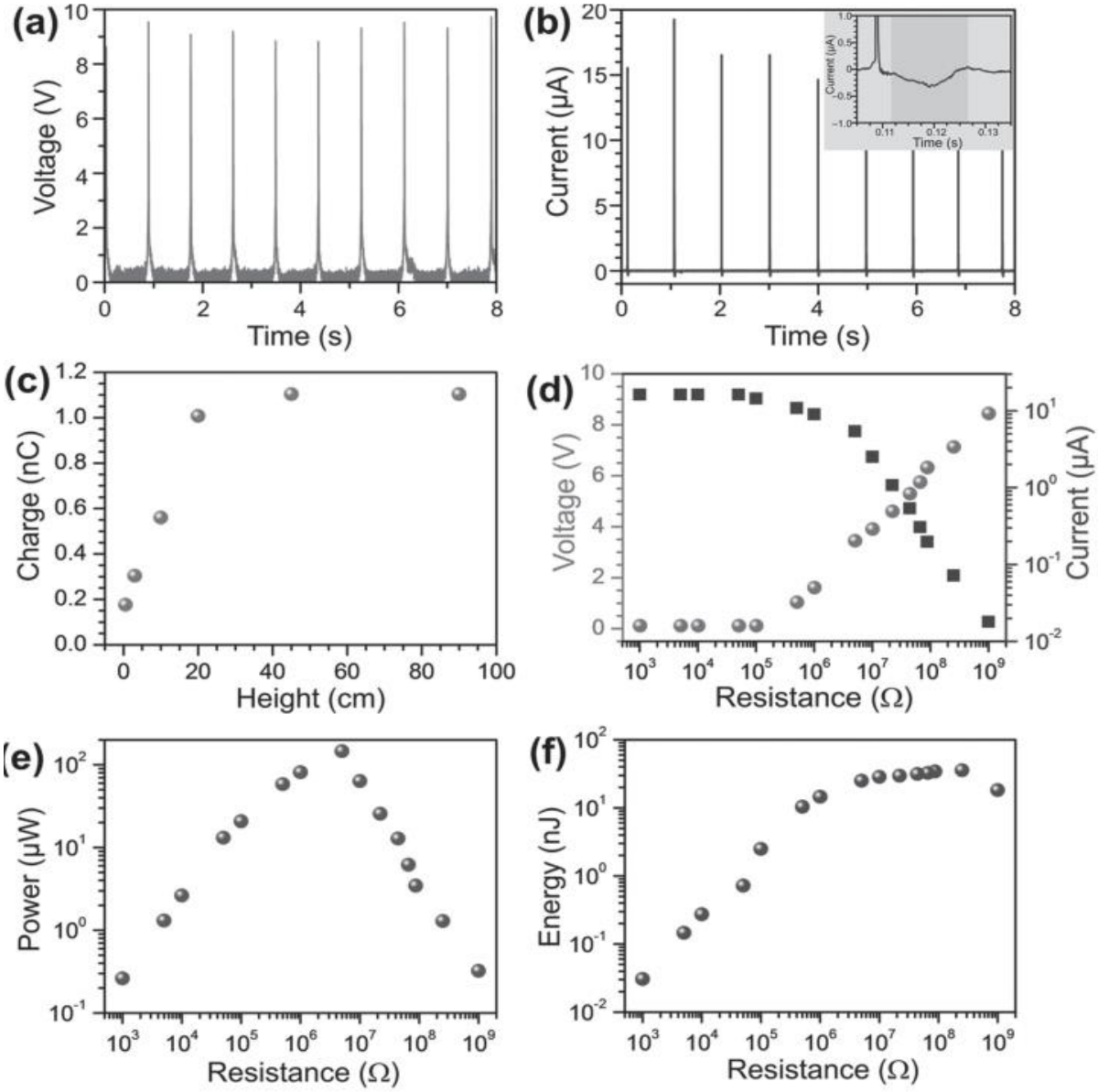

Fig. 2.6. Analysis of output voltage, current, induced charge and power output against different load resistance. [27] Copyright Advanced materials 2014.

2.2.2. Free standing mode TENG

Except single electrode mode TENG another fixed electrode based TENG is freestanding mode TENG. A typical example was proposed by Zhu et. al. [28] for harvesting water wave energy by using hydrophobic thin film. For this purpose, FEP thin film was used and the structure is shown in fig. 2.7. The practical application is shown in fig. 2.8 for the output current and voltage.

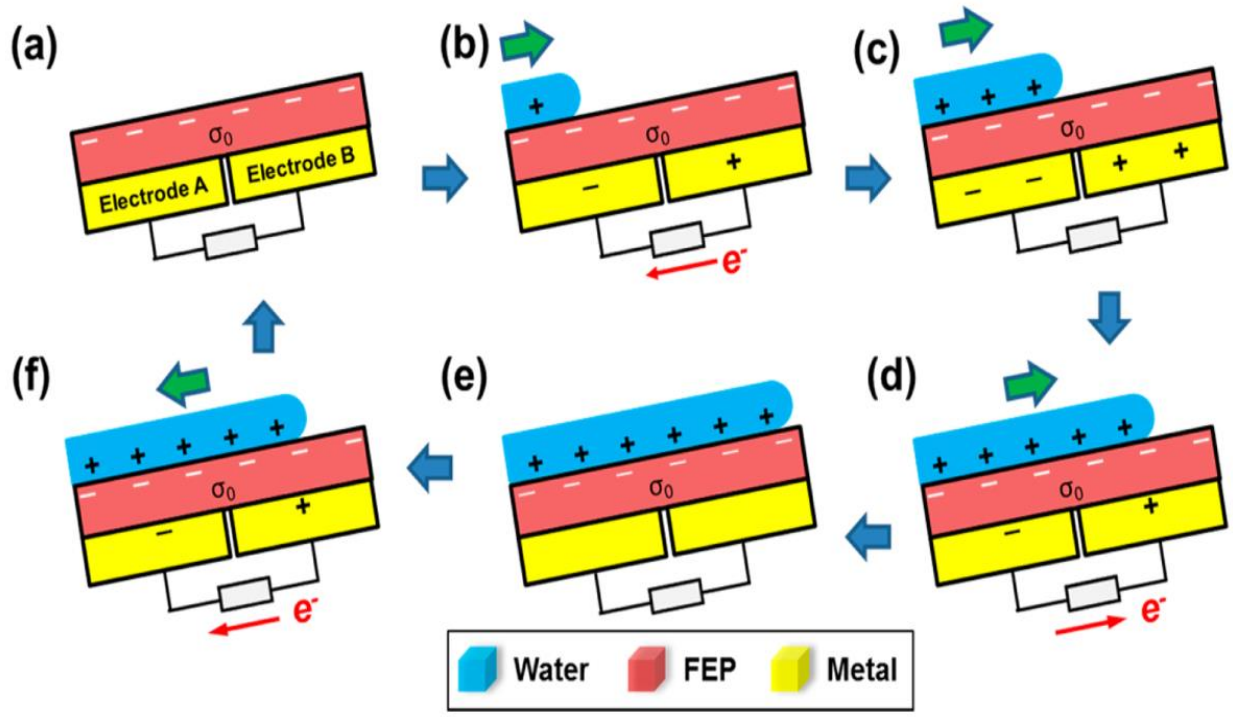

Fig. 2.7. Free standing mode solid-liquid TENG working mechanism using the FEP thin film and water. [28] Copyright ACS Nano 2014.

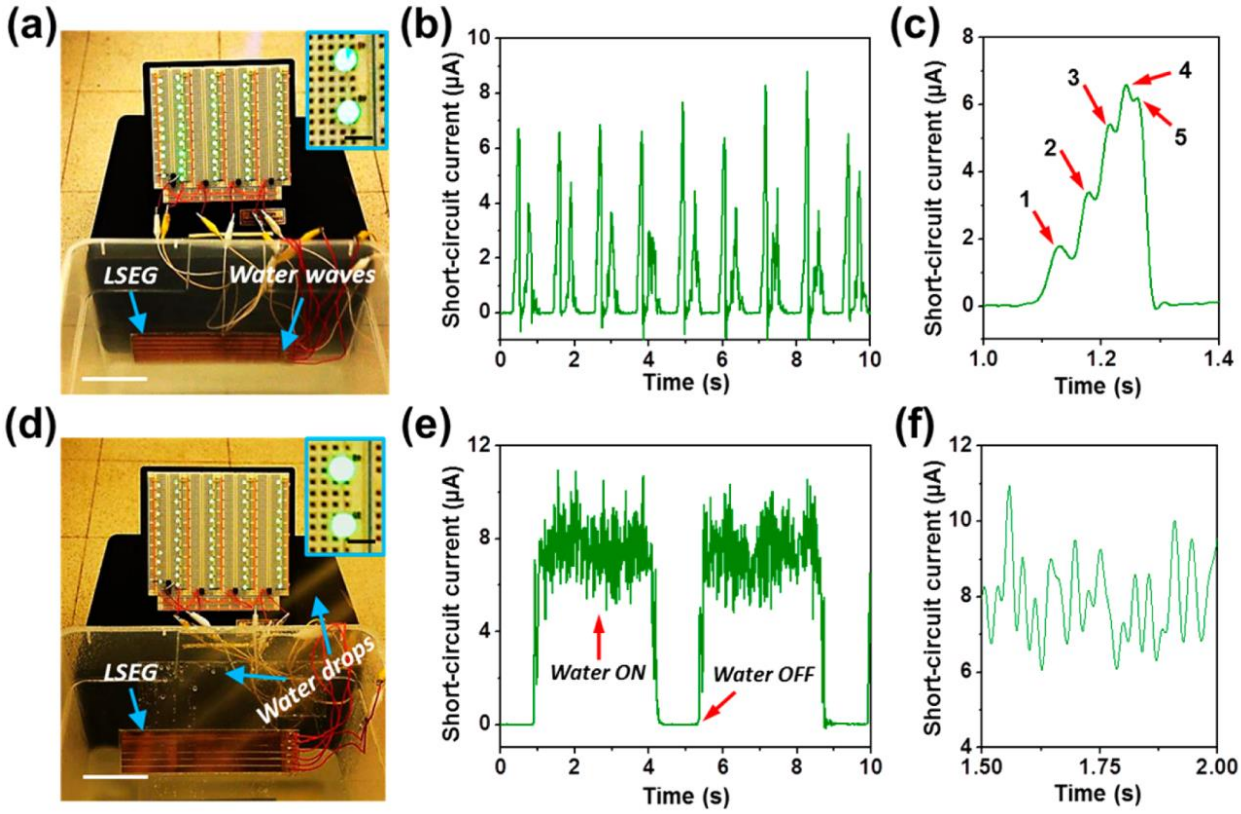

Fig. 2.8. Short circuit current generation with water wave and continuously fallen water droplets. [28]

CHAPTER 3

TENG FOR MEMS AND PIPE FLOW

3.1. Solid-Liquid TENG as potential energy harvester and transducer

Recently, Solid-liquid TENG has enormous applications in the field of Microelectromechanical (MEMS) module and pipe flows. Small volume of liquid can bear a significant message in the field of nanotechnology field. Taking the advantage of TENG, accurate results now can be obtained in cost effective way. In the MEMS technology, mechanical sensors are in vogue to collect the information from small amount of droplet such as concentration of the salt content in the droplet, living cell sorting out from the micro-organism, blood cell counting. With the advent of TENG, now the above phenomena can be realized from the interaction of the liquid with thin polymeric surface. When the tiny droplet comes over the polymeric film, in the attached electrode there causes imbalance of free electrons between the electrode and the ground after the separation of droplet from the thin film surface. Following the trend, flowing liquid in small conduits or channels can be the most accessible forms of energy in our daily life, from blood flow in veins and arteries, Xylem and Phloem in plants and capillary flow of water in the pores of the earth soil to the industrial heat exchanger or engine cooling device. Today's advance technologies like miniature sensors, fluidic actuators and cooling system in the integrated electronic device also control and manipulate the fluid flows [28]. Indeed, the flow of the working fluid in channels or tubes are linked with the significant functional elements specially pumping and actuating events which influences the dynamic properties of the fluids such as, pressure profile, velocity. [29]. These combined effects cause the various kinds of transportation techniques of the physiological liquids, chemical solutions, drug delivery, lab on chip experiments following different flow patterns like steady flow, wavy flow, peristaltic flow [30],

periodic flow of air and water as droplet [31]. Harvesting energy along with micro-nano sensing from these regulated flows can be promising future technology. Some nano-generators and transducers have already been reported based on electrokinetic behavior of pressure gradient induced steady flow in small tubing and rectangular channels [32-35].

3.2. Prospect of TENG in pipe flow

Demonstration of triboelectricity in pipe flow is very obsolete concept. But utilizing the phenomena as a transducer and energy harvester is a new technique. Lin et.al. [29] proposed a energy harvester from the continuous flow of water through the pipe. For this purpose, MoS_2@PDMS composite film was attached in the inner surface of the pipe and for the output signal Cu adhesive tape was used. From the fig. 3.1, it is shown that while utilizing the fifth cell of the tube, the voltage was obtained around 30 V. The current density was also achieved max 7 mA/m^2 for the maximum distance of 40 cm from water inlet to the outlet.

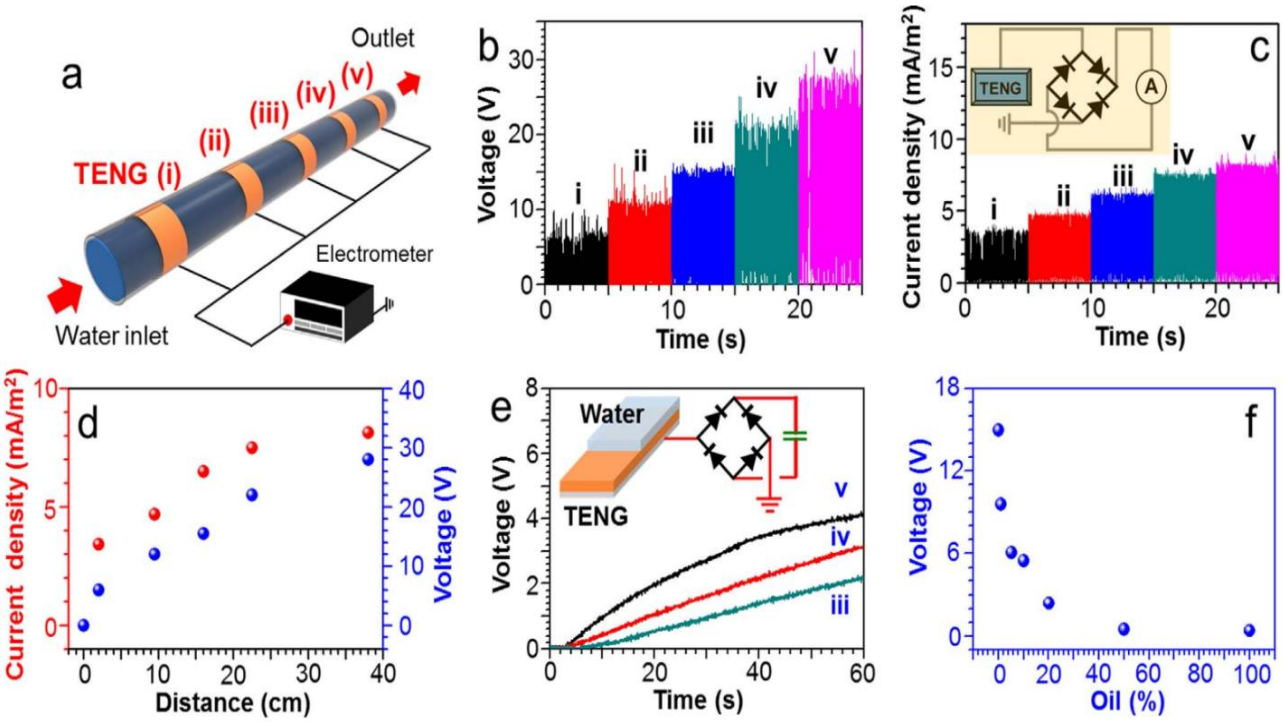

Fig. 3.1. Experimental result analysis of the pipe based TENG using five TENG cells. [29] Nano Energy 2016.

3.3. TENGS in MEMS device

Besides energy harvesting, triboelectric nanogenerator has a significant role in MEMS devices as transducing element. Till now, a great deal of sensor modules has been reported like P^H sensor, concentration sensor etc. In this context, Zhang et.al. [30] has reported a streaming potential based direct current generator for self-powered sensing. For this purpose, PDMS based MEMS device were fabricated using photolithography process and solutions with different PH values have been passed through the channel to realize the electrical output in the external circuit. As shown in fig. 3.2 the device has shown voltage output for various PH values. For the PH value of 12 the voltage was obtained around 20 mV and for the value of 5, it was about 70 mV. The results were verified with the traditional PH sensor and proved to be highly precise.

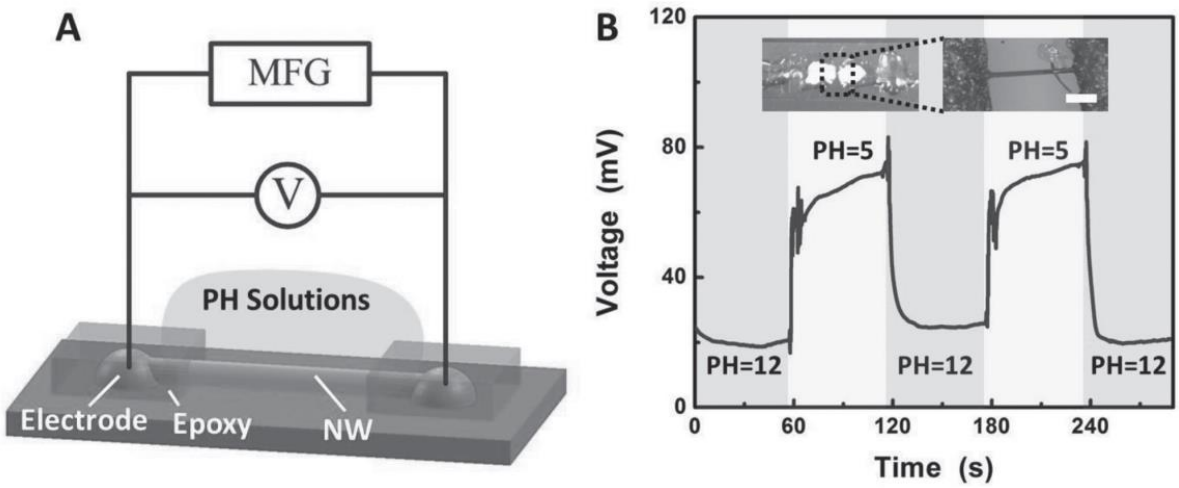

Fig. 3.2. PH analysis of different liquid flowing as a droplet through the PDMS microfluidic channel.[30]. Copyright Adv. Mat. 2015.

3.4. Objective of the current research

From the above discussion, my research motivation has aimed to the two directions: (1) Investigation of hydrodynamics effect on the energy generation during fluid-polymer thin film interaction (2) Utilizing the MEMS technology to harness energy from droplet and use the output signal to realize the certain parameters of the machineries. To deal with first direction, I've investigated on the harvesting energy from peristaltic flow which is unsteady flow in nature and mimics the physiological flow of fluid like blood from cardiac pumping. The second direction has dealt with the PDMS based MEMS device to realize the frequencies and pressure rotary actuators. According to the context, Chapter 4 and chapter 5 has been entitled as follows:

Chapter 4: Harvesting Liquid Stream Energy from Unsteady Peristaltic Flow Induced Pulsatile Flow-TENG (PF-TENG) Using Slipping Polymeric Surface Inside Elastomeric Tubing.

Chapter 5: Self-Powered Flexible PDMS Channel Assisted Discrete Liquid Column Motion based Triboelectric Nanogenerator (DLC-TENG) as Mechanical Transducer

CHAPTER 4

PERISTALTIC FLOW BASED TENG

In this chapter, a liquid-solid TENG is proposed utilizing the peristaltic flow of liquid inside the silicone elastomeric tubing that mimic the cardiac pumping of the blood through elastic arteries and veins causing peristalsis. Considering the discrepancies with the other flow generators [31-35], Peristaltic flow can be potential candidate to continuously harvest energy from the liquid stream. Until now, this significant flow dynamics has been reported by numerous literature reviews [36-40]. But there are no reports relating to harness energy from this pulsatile one-dimensional flow type.

4.1. What is peristaltic flow?

Generally, Peristalsis means a circumferential progressive wave of contraction or restitution that propagates along the elastic tubing, capillary or vessels. The pulsatile flow type originated from the squeezing and releasing of the elastic muscles is a major technique of the physiological fluid flow [41,42]. The peristaltic mechanism involves in the vasomotion of the blood vessels i.e. venules, arterioles, transport of lymph in the lymphatic vessels, urine transport from the kidney to the bladder, valve less motion of the cardiovascular system in embryonic [43-45]. Since the first development of heart-lung machine, today the peristaltic flow has shown its promising applications in biomedical, industrial, agricultural and wastewater treatment applications. For example, these pumps are used to convey viscous fluid in the printing industries, peristaltic transport of noxious fluid in the nuclear plants, biological cell sorting in lab on chip experiment [46]. The use of peristaltic pumping has become versatile as it facilitates the sterile fluids to convey without further contamination from the mechanical components. From this point of view, generating

electricity from this flow type is a novel approach in the widespread field of nano-energy harvester.

4.2. Material descriptions and methods

To develop the PF-TENG cell, elastomeric silicon tubing with 4 mm inner diameter and 1mm thickness was chosen for liquid flow. As the solid tribomaterial, the mpPVDF membrane with 50 µm thickness and 0.45 µm pore size was bought from Sigma Aldrich. The mpPVDF membrane provides high surface area to volume ratio through its porous network comprises of interconnected nodes and fibrils. Hydrophobicity of the PVDF membrane was determined through contact angle analysis by using DSA 100 Gomiometer (error $\pm$ 1%) following sessile droplet method (Droplet Vol. 5 µL). The surface morphology of the pristine mpPVDF and post experiment has done using HITACHI cold FE-SEM microscope which operates at 10 KV. The FE-SEM image of the pristine mpPVDF represents the micro porosity as shown in fig.4.1(a). The value of the contact angle in the inset image of fig.4.1(a) shows obvious hydrophobicity, attributed to the nanostructure of the membrane. The commercial purpose Aluminum tape was used as an electrode.

The mpPVDF membrane was prepared with the dimensions of l=3 cm, w=1 cm and attached to an aluminum (Al) tape for use as an electrode, fig.4.1(a). It was then attached to the inner wall of a silicone tube using double-sided tape to make the PF-TENG cell, as depicted in the real photograph in fig.4.1(c). The surroundings of the electrode cell were sealed properly with extended double-sided tape to prevent the leakage of the working fluid to the Al electrode. The PF-TENG cell was attached inside the tube as semicircular shape as presented in fig. 4.1(b). So, the effective contact area (wetted area) of the liquid stream with the PF-TENG is $A_w = \pi ab = 0.000942 m^2$.

Tap water from general sources are highly variable in their mineral contents and some contribute appreciable amounts of certain minerals due to natural conditions (e.g., Ca, Mg, Se, F, Zn), intentional additions (F), or leaching from piping (Cu). We obtained tap water from a commercial source (K-water, S. Korea) [47], which contains moderate mineralization with 200 to 700 mg/L of Na^+, Mg^{2+}, and Ca^{2+} ions, as well as trace amounts of F^-, Cu^{2+}, Zn^{2+}, and K^+ ions. The tap water also forms carbonic acid groups (HCO_3^- and H^+) with the presence of atmospheric CO_2 as it is exposed to open air. DI water was used from our research lab by double distilling and has a resistivity of 18 MΩ.cm at 25 ^oC.

A simple circuit was designed to evaluate the load characteristics as well as to show output performance of the PF.TENGs by charging the capacitor. A Keithley Source Meter (Keithley DMM7510) was used to analyze the output voltage and short-circuit current (I_{sc}), fig.4.2(d). The generated voltage was measured with 10 MΩ internal load resistance.

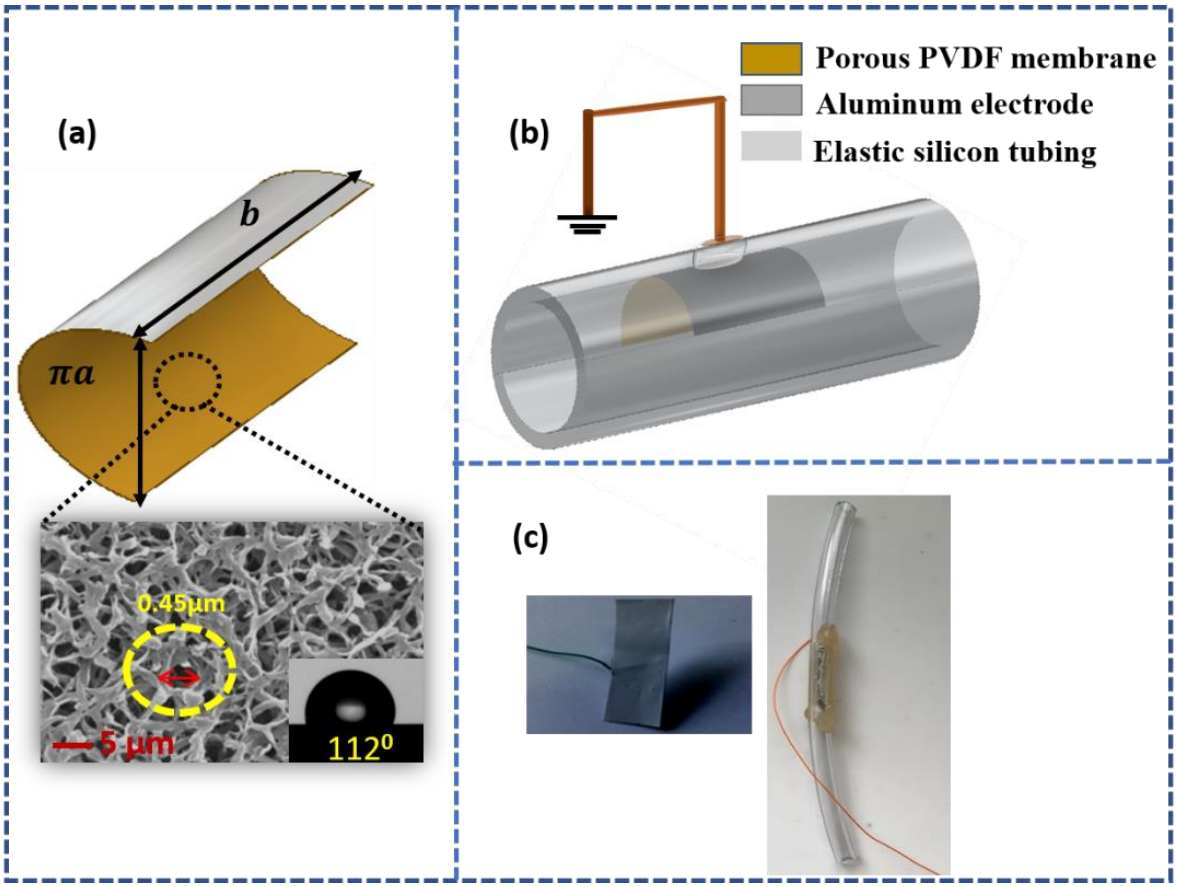

Figure 4.1. (a) The CAD model of the PF-TENG cell with FE-SEM image of the mpPVDF membrane(Inset image: contact angle), (b) Schematic of the elastomeric tubing with PF-TENG cell attached, (c) Real photograph of the PF-TENG

4.3. Material characterization using FE-SEM

The FE-SEM images are presented to analyze the surface morphological changes in the Pristine PVDF film, post-experimental PVDF film interacting with the Tap water and DI water respectively as shown in the fig.4. In the pristine PVDF, the pore sizes appeared at 0.45 µm fig.4.2(a), while the gap is reduced more after interacting with PF.Tw-TENG, fig.4.2(c) over PF.DIw-TENG, fig.4.2(b). The contact angles were also increased form the Pristine mpPVDF to the PF.Tw-TENG in the order of

112<118<121^0 and thus increase the hydrophobicity. This is due to the fouling of the dissolved ions present in tap water in the mpPVDF membrane matrix network. As a result, the polymeric fibrils network is stretched that facilitates the increased contact surface area as well as high charge density compared to commercially available smooth film. The hydrophobic nature has supported the long-term efficiency of the proposed device with stretched morphological network of the surface.

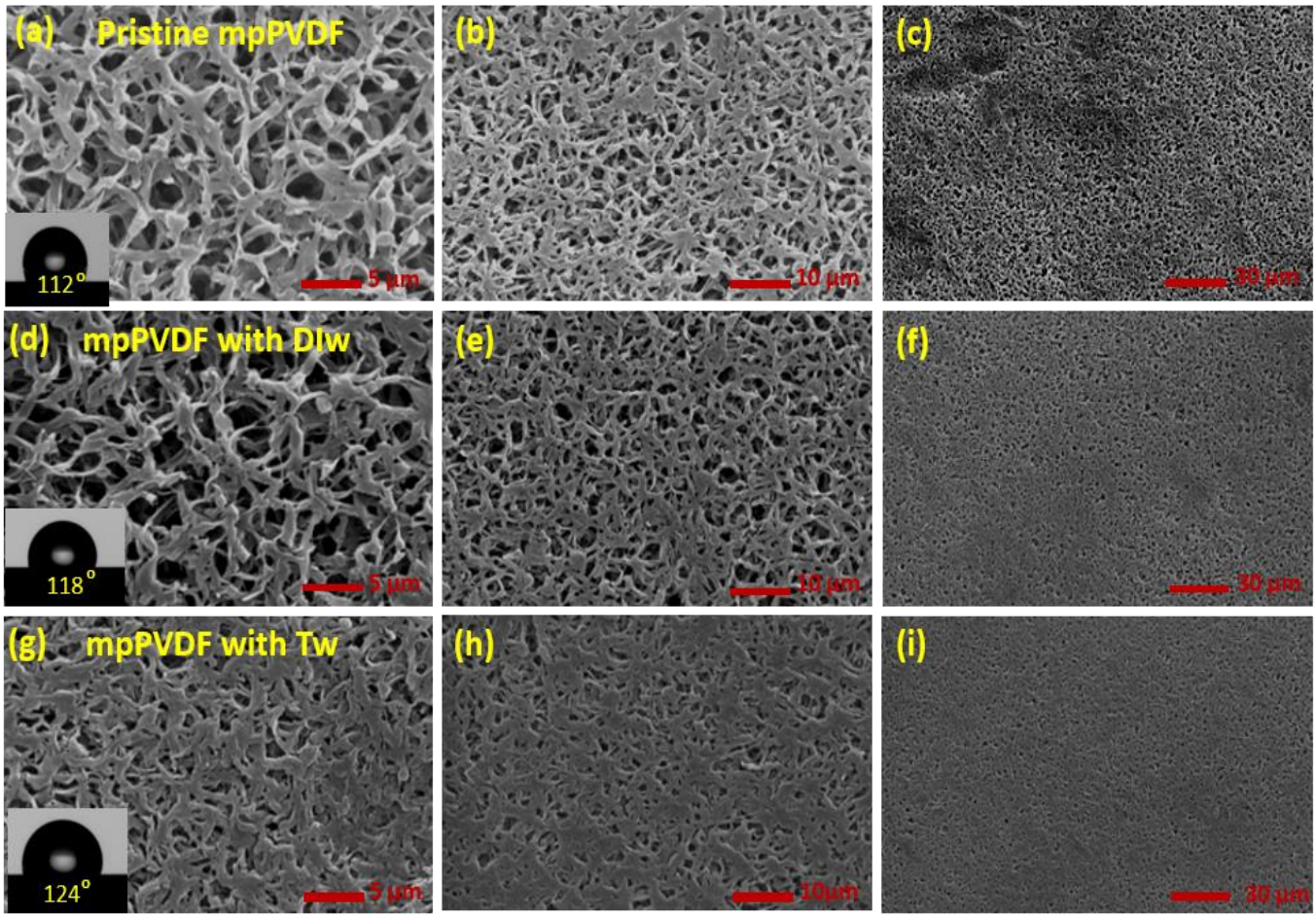

Figure 4.2. FE-SEM images of the (a,b,c) Pristine mpPVDF, post experimental image (d,e,f) mpPVDF with DIw, (g,h,i) mpPVDF with Tw at different scale (Inset: Contact angle)

4.4. Experimental setup

To generate the pulsatile flow, a peristaltic pump with the three-roller configuration (Ecoline VC-360) has been used in the experiment, fig.4.3(a). The long go through silicon tubing with the PF-TENG cell as described in the material section has used for the fluid passage that continuously circulating the 500 ml volume of working fluid, fig. 4.3(b). The whole experimental setup has shown in the Fig. 4.4.

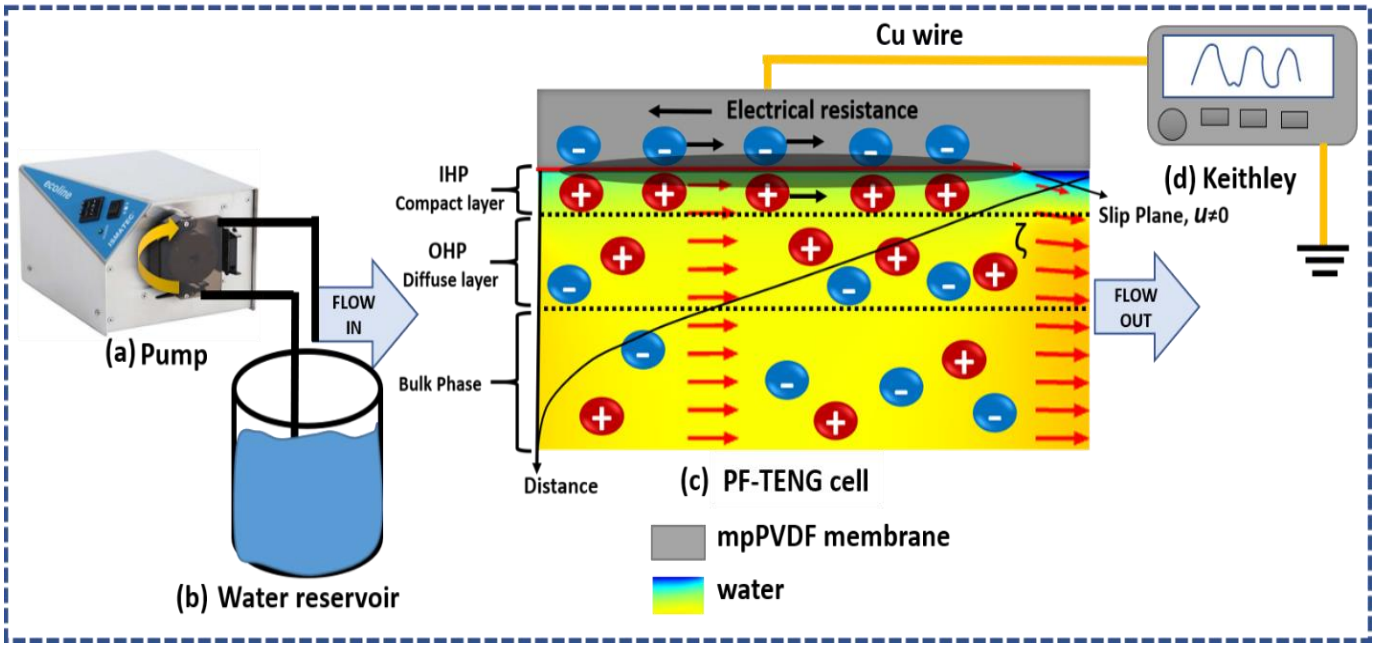

Fig. 4.3: Schematic diagram of the experimental setup showing the (a) Peristaltic pump, (b) 500 ml beaker with filled liquid (c) FP-TENG cell showing the EDL=IHP+OHP formation at the solid-liquid interface and the decrease of the zeta potential from the IHP to the bulk phase of the liquid. (d) Electrometer.

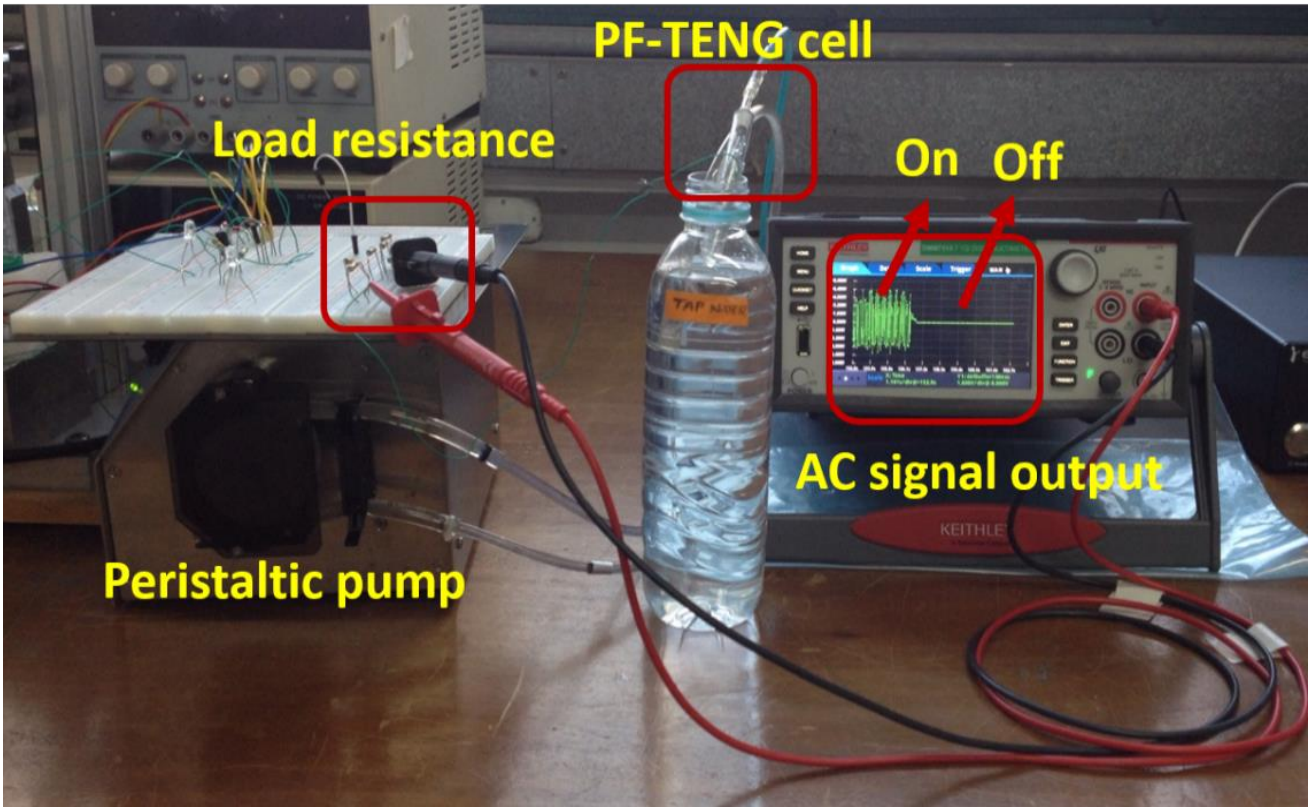

Fig. 4.4: Illustration of the PF-TENG experimental setup

4.5. Intrinsic AC charge generation

To quantify the charge generation mechanism in the PF-TENG cell from the liquid stream, a mathematical modelling that coupled the hydrodynamics with the electrostatic induction in the PF-TENG solid-liquid interface has explained with the help of electrical double layer formation according to Guoy-Chapman-Stern layer model [48]. When the liquid starts flowing through the silicon tubing, at the tubing solid surface the immobilized Silanol group (Si-O-H) becomes protonated and negatively charged and screens the opposite counterions of the liquid at the solid liquid boundary. Due to the no slip (U=0) boundary condition at the wall, the highly concentrated ions are immobile in the solid-liquid interface though the working fluid flows. The hydrophobic properties of the mpPVDF membrane provides slip condition (U≠0) at the liquid-solid interfaces which facilitates highly concentrated

ions to be mobile in the range of slip plane and solid boundary and enhances the liquid flow velocity. [49-50] The ions in the slip plane maintains the same velocity with the liquid flow over the mpPVDF membrane.

Upon contact with the liquid, the PVDF surface, due to its CF_2 group has become highly electronegative so thus attracting the positive counterions following the electrostatic induction and triboelectrification. This phenomenon causes the formation of EDL in the slip plane. The EDL consists of Inner Helmholtz Plane (IHP) where the positive counterions can move tangentially along the flow direction over the mpPVDF membrane and the other one Outer Helmholtz Plane whereas the mobile co-ions and the counterions can exists together as shown in the schematic diagram of the fig. 4.3(c). In the IHP, the movement of the counterions are influenced by the general hydrodynamics of the liquid stream in the pipe flow. This counterions can move tangentially along the slip range of the boundary wall but shows reluctance to be accumulated in the OHP or in the bulk liquid. In case of OHP, the ions with the opposite polarities can go to the bulk liquid. As water is viscous incompressible Newtonian liquid, so for the peristaltic flow at the PF-TENG cell-liquid interace, the continuity and Navier Stokes equations also hold good and can be modified for the ion's movement in the IHP [51,52].

$$\frac{\partial \rho}{\partial t} = \nabla \cdot (\rho \upsilon_{fluid}) = 0 \qquad (1)$$

Where, ρ and υ_{fluid} are the density and velocity of the fluid respectively.

The modified Navier-Stokes equation

$$\rho \frac{\partial \upsilon_{fluid}}{\partial t} + \rho(\upsilon_{fluid} \cdot \nabla)\upsilon_{fluid} = \nabla \cdot [-\rho I + \mu(\nabla \upsilon_{fluid} + \left(\nabla \upsilon_{fluid}\right)^T)] + F_n \qquad (2)$$

Where, F_n is the body force vector imposed on the liquid. In our case, the body force is the applied electrostatic attraction force in normal direction between the electrons of the mpPVDF and the positive charges in the IHP. According to the Guoy-Chapman [53], this attraction force can be in the flowing form

$$F_n = \frac{\left(qE_n = A_p\sigma^2\right)}{(\varepsilon_0\varepsilon_1)} \tag{3}$$

Where, q is the electric charge, A_p is the effective contact area, σ is the surface charge density, ε_0 and ε_1 are the dielectric permittivity of the vacuum and the liquid. At the PF-TENG-liquid interface, the liquid will become positively charged due to high dielectric constant according to Cohen's rule [54]

$$\rho = 1.5x10^{-5}(\varepsilon_1 - \varepsilon_2\ ) \tag{4}$$

Where, ε_2 ,ρ are the dielectric constant of the mpPVDF and the space charge density respectively. The Debye characteristic length at the IHP can be expressed by,

$$\lambda_D = \frac{\xi\varepsilon_0\varepsilon_1}{\sigma} \tag{5}$$

Where ξ is the Zeta potential as represented in fig. 4.3(c), that gradually decreases from the IHP to the bulk phase of the liquid. The shear stress τ_w of the liquid imposed on the wall can be written by [55]

$$\tau_w = \frac{2\mu\upsilon_i}{R = \lambda_D} \tag{6}$$

In the eqn. (6), the υ_i is the ion velocity that is equal to the υ_{fluid}, at the IHP and the radius of the pipe R can be replaced by the Debye Length. So, the implied shear force and the derived ion velocity can be expressed by eqn. (7) and (8) respectively.

$$F_s = A_p\tau_w = A_p\mu\frac{2\upsilon_i}{\lambda_D} \tag{7}$$

$$\upsilon_i = \frac{\tau_w \lambda_D}{2\mu} \tag{8}$$

Due to the slip boundary condition applied on the over the mpPVDF membrane the ion velocity υ_i will be multiplied by the factor of $(1+\frac{b}{\lambda_D})$ [56], where b is the slip length. So, the ion velocity becomes

$$\upsilon_i = \frac{\tau_w \lambda_D^2}{2\mu(\lambda_D + \mathrm{b})} \tag{9}$$

The static friction force in the solid mpPVDF that reacts oppositely to the shear force is equal to the F_n multiplied by the friction coefficient μ_s following Amonton's law of static friction

$$F_f = \mu_s F_n \tag{10}$$

Indeed, the ions start to slip against the solid boundary of the membrane when $F_s > F_f$. On the other hand, in the solid surface the electrons are dragged by the shear force of the ions, but the velocity is retarded due to the electrical resistance of the solid. During this time, the momenta are conserved for both the ions and electrons at the interface. The electrons are lagged of behind the ions causing relative distance consequently velocity difference which induces the potential difference in the interface and short circuit current in the external load. From the solid-state physics, the Drude model is adopted for the electrons in solid surface

$$\frac{d(m\upsilon_e)}{dt} = \frac{-m\upsilon_e}{\tau + qE_{ext}} \tag{11}$$

Where, υ_e , τ, qE_{ext} are electrons velocity, Drude relaxation time and applied external field. In the model, it is assumed that, the electrostatic attraction is strong

enough that the electrons are dragged by the accelerated ions in the IHP. As the external applied is zero [57], so the eqn. (10) reduces to

$$\frac{d(mv_e)}{dt} = \frac{-mv_e}{\tau} \tag{12}$$

The momenta are conserved across the interface for the electrons so,

$$\frac{F_s + d(mv_e)}{dt} = 0 \tag{13}$$

Combining eqn. (10) and (11) the electron velocity becomes as follows

$$v_e = \frac{F_s \tau}{m} \tag{14}$$

Now, the amount of net induced charges in the mpPVDF membrane due to the electrostatic potential caused by the relative distance between the ions and electrons

$$Q_s = \sigma_o S = \sigma_0 wx \tag{15}$$

The induced net electric current in the solid surface is given by

$$I_s = \frac{dQ}{dt} = \sigma_0 w \frac{dx}{dt} = \sigma_0 w \Delta v = \sigma_0 \pi a (v_i - v_e) \tag{16}$$

The resultant mpPVDF surface electric potential due to the electrical resistance, R and electric current is

$$\psi_s = I_s R = \frac{I_s}{bK_s} \tag{17}$$

Where, b is the length of the mpPVDF and K_s is the surface conductivity.

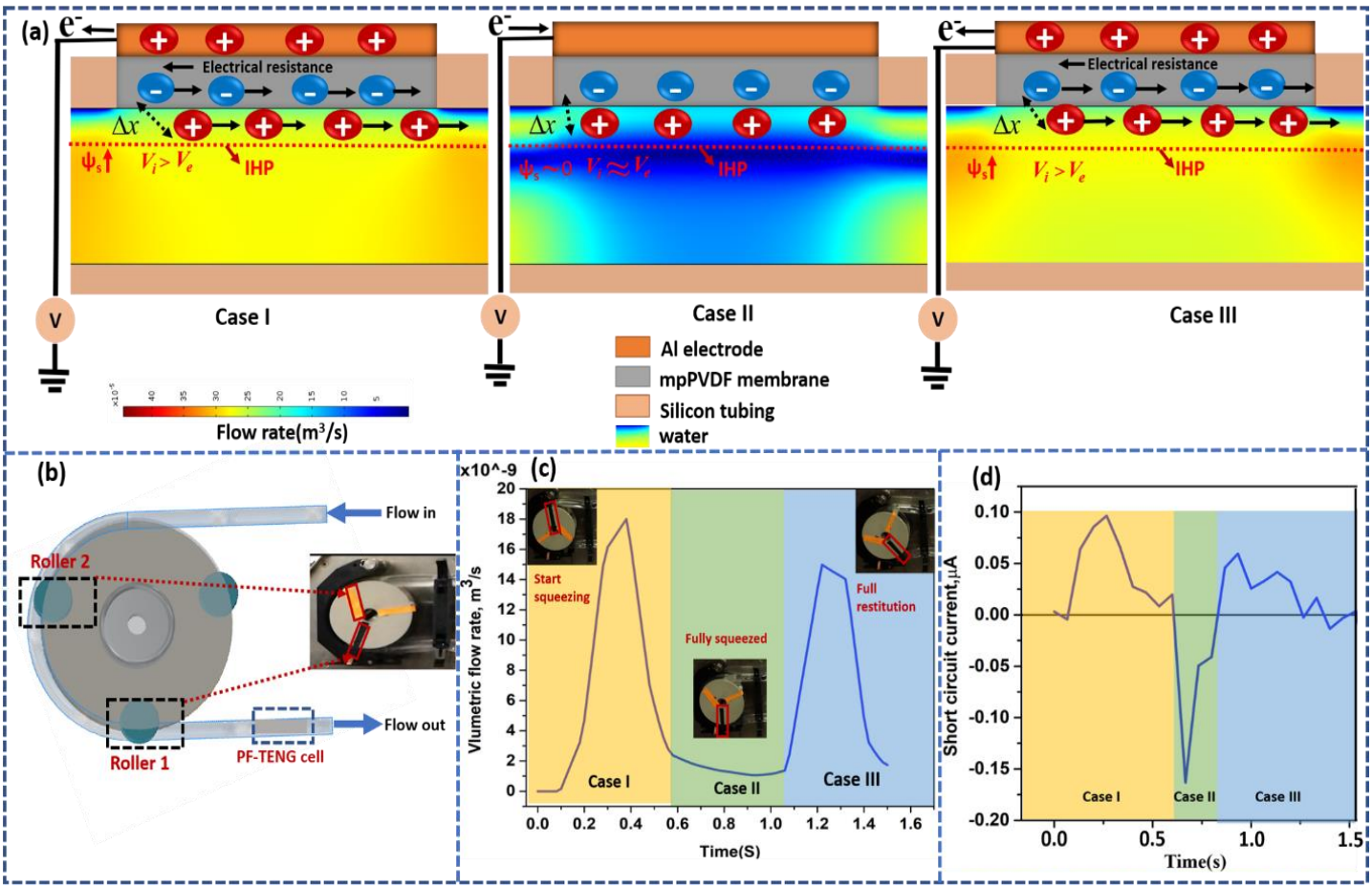

Figure 4.5. Intrinsic AC charge generation during squeezing and restitution of the roller 1 to deliver the fluid at one pump cycle of 1.4s. (a) Charge distribution at different cases in solid-liquid interface and the Al electrode. (b) Schematic of the peristaltic pump showing roller configurations and the position of the PF-TENG cell at the outlet of the flow; at the pump speed of 40 rpm (c) Outflow of the fluid at three different case for roller 1 obtained from COMSOL simulation. Inset (Real photograph of the three different condition of the roller 1) (d) The short circuit current peak obtained from the experiment in three cases for the squeezing and relaxation process for the roller 1.

Based on the derived eqn. (9), (14) and (17) for the ion velocity, electron velocity and surface potential of the mpPVDF membrane respectively, the triboelectrification due to the pulsatile flow over the PF-TENG cell can be explained. For this purpose, a COMSOL simulation model describing the velocity distribution due to peristalsis over the slip surface that contribute to the AC signal generation obtained from the experiment in half revolution index of single roller among the three rollers of the pump has represented in fig.4.5. In the three-roller peristaltic pump arrangement. as shown in fig. 4.5(b), among three rollers, the two rollers are always in contact with the elastic tubing in one half cycle of any roller. The liquid entrapped between roller one and roller two is called the dead volume [58]. So, to elucidate the mechanism, here, the roller one is considered as the functioning element to deliver the fixed volume of liquid at the outflow over the PF-TENG cell through one half cycle of squeezing and restitution of the elastic tubing fig.4.6 [59]. Due to the squeezing and restitution, a circumferential progressive wave following the distorted sine curve with the up and fallen crest along positive Y-axis propagates along the tube which is also induced in the liquid flow and specially influence the movement of the ions in the IHP over the mpPVDF membrane. The mechanism of the obtained AC signal generation can be divided in three process of the roller one, (i) Squeezing, (ii) fully squeezed and (iii) full restitution. During squeezing the ions are accelerated

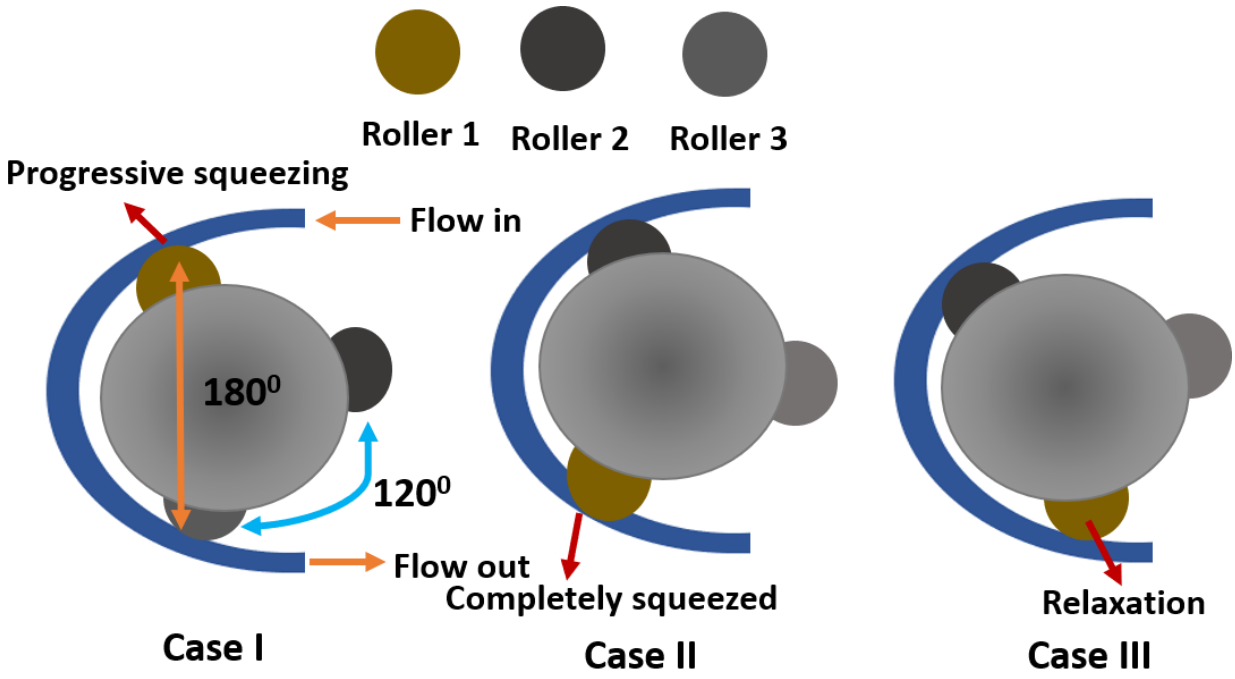

Fig. 4.6: The flow processes at three cases with respect to positioning of the roller 1. Case I: Working fluid is despensing downstream, Case II: Flow rate decreasing causes liquid to cease. Case III: Liquid is dispensing again in downstream

and the shear force of the flow can overcome the electrostatic force. As a result, there is an electrostatic potential difference between the negative charges of the mpPVDF membrane and the positive ions in the slip plane which causes the generation of positive peak of the AC signal in the external load. While in fully squeezed condition the ions tend to decelerate or ceased slightly with the flow thus the electrostatic potential difference is also reduced following the process causing the negative peak in the external circuit. On the other hand, in the restitution process by the roller one, at the instantaneous moment, the dead volume pushes forward the fixed volume to be dispensed at the outlet which again results in acceleration. The accelerated ions cause the electrostatic potential difference in the slip plane again and positive peak component of the AC signal is found. The whole process can be further summarized

easily with the help of the flow dynamics of the peristaltic process that relates the above derived eqn. 16 for the short circuit current generation due to the relative velocity between the positive ions and negative charges of the mpPVDF membrane with the obtained current signal as described in the fig. 4.5(d). For our simulation, at the pump speed of 40 rpm with the flow rate of 70ml/min, the engaging and disengaging time for the roller one has counted 1.5 s from the experimental setup. The three cases are discussed in fig. 4.5(a), 4.5(c) and 4.5(d) to represent the charge generation relating the change of the flow rate with the generated current peaks. When the liquid is flowing, the squeezing starts by the roller one, in the PF-TENG-liquid interface due to the positive displacement of the fluid , case I: Δx increases, $\upsilon_i > \upsilon_e$, ψ_S also increases, the excess negative charges in the Al electrode will go to the ground and positive peak has come out. During completely squeezed condition, the liquid in the downstream tends to decelerate and cease slightly, as the volume is minimized suddenly by the roller one, so $\Delta x \approx 0, \upsilon_i \approx \upsilon_e$, ψ_S tends to zero for case II, therefore, to maintain the neutrality, the electrons will move again to the Al electrode from the ground and negative peak was found. During the full restitution, as the volume is maximized, the trapped volume between roller one and roller two now displaces the liquid again in downstream, as depicted the case III of fig. 4.5(a), 4.5(c) & 4.5(d) similar phenomena like case I. As it can be predicted from the fig. 4.5(c) that, with the increment of the pumping speed, the length of the duration for case II will be shortened and with the higher speed tends to become a peak point. The corresponding negative peak are will also be shorten correspondingly. Here, it is noted that, the ideal peristaltic pump always propagates the progressive wave of equally distributes sharp and fallen crest in the tubing along with the associated liquid, so from this point of view, the AC signal peak should follow the same properties. As we know, no mechanical device has come up with the 100% ideal

properties and the parameters like elasticity of the tubing and thickness may also cause the distortion in the ideal sine wave. So, the signal can fluctuate over every pump cycle as the rate of acceleration and deceleration is not equal all the time. The reason can be more conspicuous from the simulation result as shown in fig. 4.5(c), that has obtained from the pump parameters and the properties of the tubing, has shown the distortion from the ideal and it influences the shape of the generated AC signal from the experiment.

4.6. Application as energy harvester

The output performance of the PF-TENGs has been studied using the mechanical circulation of DI water, tap water at different pump speeds of 140 rpm, 210 rpm, 280 rpm, and 350 rpm using the 3x1 cm mpPVDF membrane. Fig. 4.7 has shown the electrical output of the PF-TENGs, the output voltage and the short-circuit current (I_{sc}). The PF.DIw-TENG produced average peak to peak values of voltage are of 7 V, 9 V, 9.5 V,10 V and the corresponding I_{sc} values are 0.38 µA, 0.49 µA, 0.48 µA, 0.46 µA at 140, 210, 280, and 350 rpm, respectively, Fig. 4.7b-d. The peak to peak values of voltage of PF.Tw-TENG at 140 rpm were 11.06 V (+5 V and -6.06 V) and generated I_{sc} was attained from -0.45 µA to 0.5 µA. When the tap water speed was increased, the output voltage and I_{sc} also showed increasing trends. In particular, at 210 rpm, 280 rpm, and 350 rpm, the generated average peak to peak values of voltage were 15.93 V, 17.29 V, 20.92 V and the I_{sc} obtained from -0.55 µA to 0.6 µA, from -0.6 µA to 0.8 µA and from -0.75 µA to 0.95 µA, respectively, Fig. 4.7a-c. The inset images of all the figures revealed consistent output of the voltages and currents. The output values from the PF.DIw-TENG were very poor compared to the PF.Tw-TENG due to their difference in conductivities. The PF.Tw-TENG showed high electrical output compared to the PF.DIw-TENG due to the presence of dissolved mineral salts at 200 to 700 mg/L (i.e. Na^{+}, Mg^{2+}, and Ca^{2+}), which are

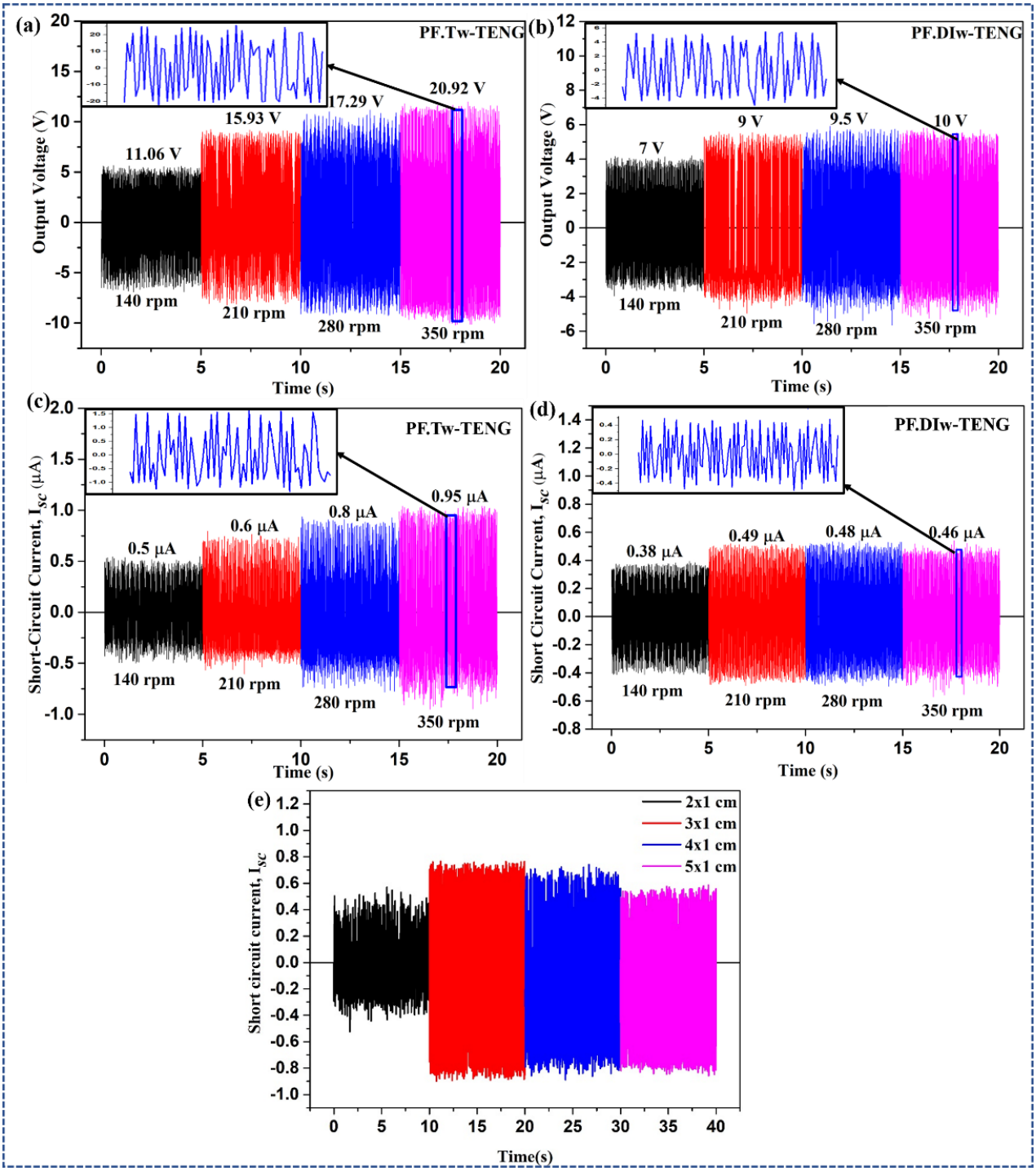

Fig. 4.7. Output voltage & short-circuit currents (I_{SC}) of PF.Tw-TENG (a & c), PF.Tw-TENGs (b & d) at variuos rpms, Inset (consistency of output signals for all

PF.TENGs), (e) short-circuit currents (I_{sc}) of the PF-TENG cell with the different mpPVDF membrane sizes at 350 rpm using tap water.

responsible for the generation of higher voltage and current at all the provided pump speeds. As it is discussed earlier in the section 4.3.1, the silicon tubing has attributed to the charge polarization due to triboelectric effect in the IHP that cause precharged state before the water entering to the PF.TENG cell. The phenomena can provide the improved efficiency of the provided TENG within small area. In this case, water potential can be assumed to be raised in the fluidic circuit but that is not enough compared to the volume of the working fluid in the reservoir. To clarify this, experiment was conducted using the reservoir water as ground and compared with the normally ground state in case of tap water as shown in fig. 4.8. From the observation, no obvious change has been occurred in the signal of open circuit voltage. In line with the above context, the realized high voltage in the external load can be solely attributed to the rapid sliding action through acceleration and deceleration of the ions in the EDL over the PF.TENG cell. The AC behavior of the generated voltage has distinguished it from the conventional electrokinetic nanogenerator or electrolytic cell whereas DC voltage with similarly generated voltage may cause water decomposition with the threshold voltage greater than at least 1.229 V. Furthermore, to check the ions effect on the performance of the as proposed device, experiment was conducted with the increased concentration of tap water. For this purpose, first we have taken the 240 ml of tap water and boiled it to the reduced volume of 160 ml to increase the concentration of dissolved ions in the open air. As we know tap water contains common volatile carbonic acid in the form of HCO_3^- and H^+. During the boiling process, the boiling has done in the open air at 120^0 C on the hot plate, and the equilibrium of the reaction ($CO_2 + H_2O \longleftrightarrow HCO_3^- + H^+$) shifts to the left and the carbonic has formed gas and escapes.

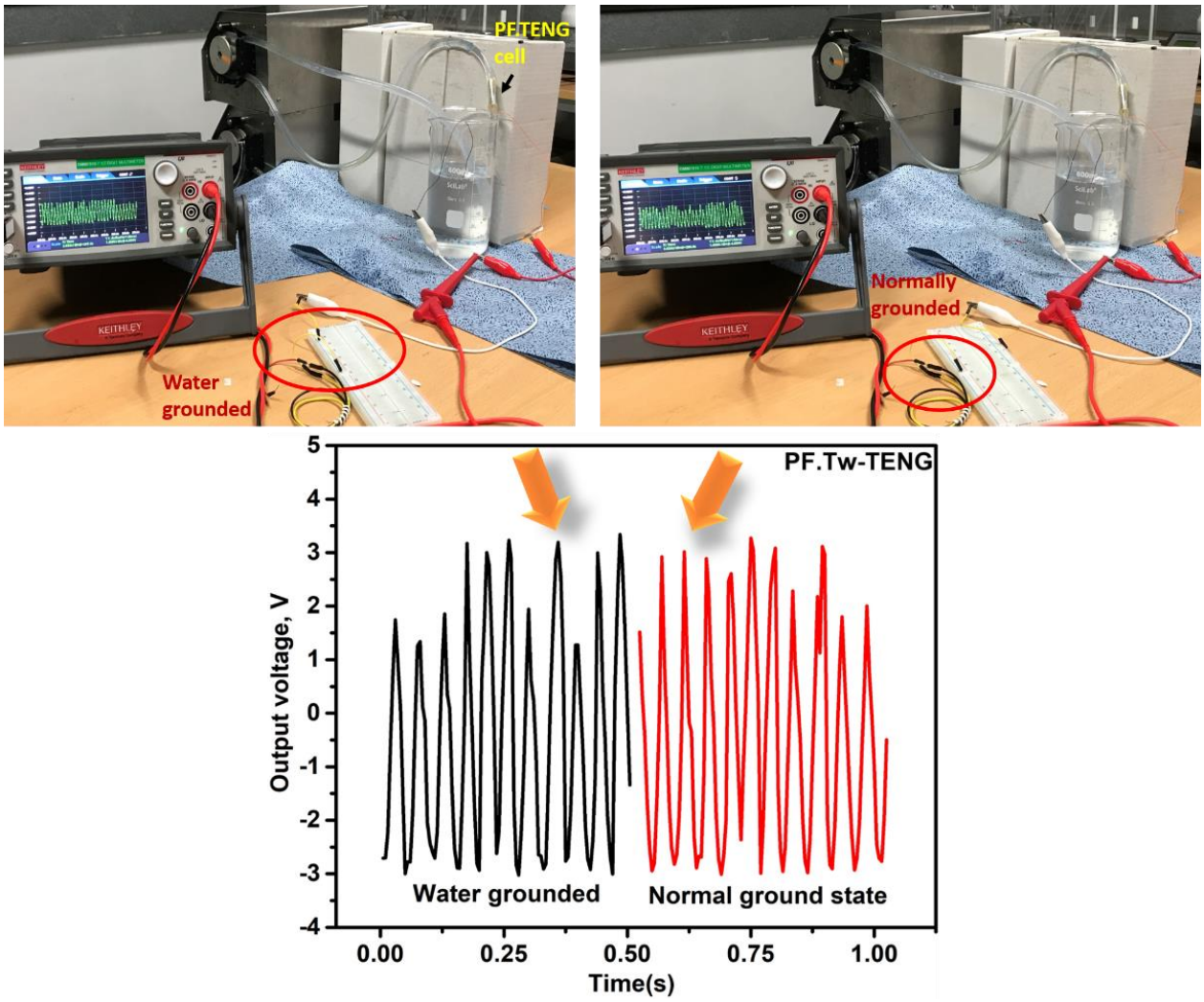

Fig. 4.8: Measured output voltage with respect to negative end grounded with working volume of tap water and with normal ground state at specific rpm.

This reduce amount of H^+ ions decrease the P^H and increase the concentration of the dissolved ions. The P^H values for DI, Tap and boiled tap water have found 5.95, 7.76, 9.62 respectively. After that, 160 ml of DI and tap water have taken respectively and experiment at 210 rpm was conducted and the comparison graph of the results has depicted in the fig.4.9. The data is now taken after the two months of the fabrication of the PF.TENG cell.

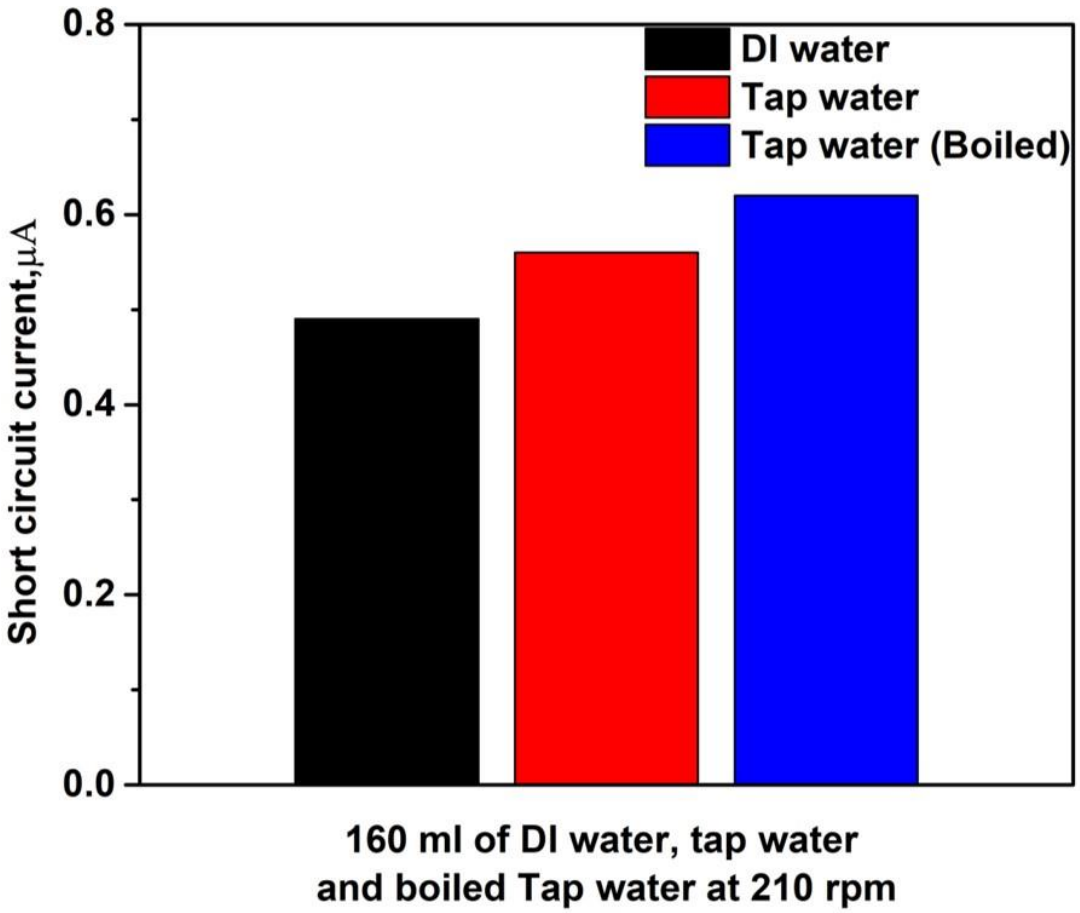

Fig. 4.9: Concentration effect on the performance of the PF-TENG

From the observation we can say that, though the H^+ ions are reduced due to vaporization in the boiled tap water but overall concentration has increased due to the dissolved ions which helps to increase the current output slightly than normal tap water. Thus, it can be said that dissolved ions can have the effect in the charge generation in the proposed system. The experiments with 1x2 cm, 1x4 cm, 1x5 cm mpPVDF membrane sizes were performed and the electrode with size 3x1 cm has shown better short circuit current as shown in fig. 4.7(e).

Fig. 4.10(a) and fig. 4.10(b) shows the maximum induced coloumb charge at different speed of the pump for DI water, tap water respectively. At every chosen pump speed,

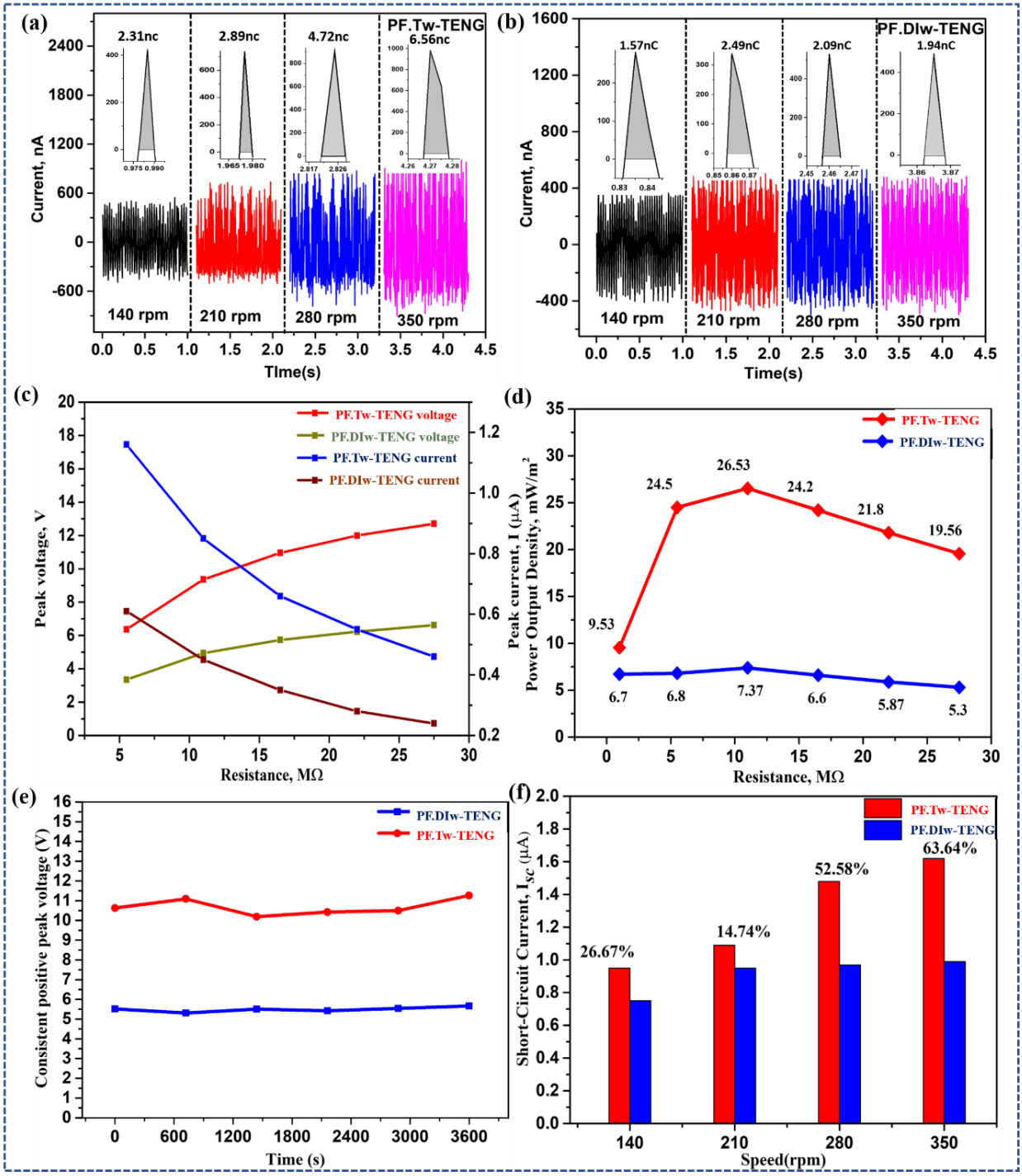

Figure 4.10. Calculation of transferred charge with the sampling time of 1s at different rpm (a) PF.Tw-TENG , (b) PF.DIw-TENG, (Inset image: Maximum transferred charges from the single peaks); (c) Power output with an external load

resistance under pulse signal input; (d) Performance characteristics of the dependent on the power output density; (e) Durability test for 1 hour; (f) Comparison of maximum short circuit currents; of all the PF-TENGs.

the sampling was done from the dataset of 1s to choose the maximum positive single peak of the current value and the induced coloumb charge is calculated by integrating the area between the X-axis and single peak value. After that, the charge transfer density was calculated by dividing the induced coloumb charge by the calculated effective contact area described in the section 5.2.2. and the method of

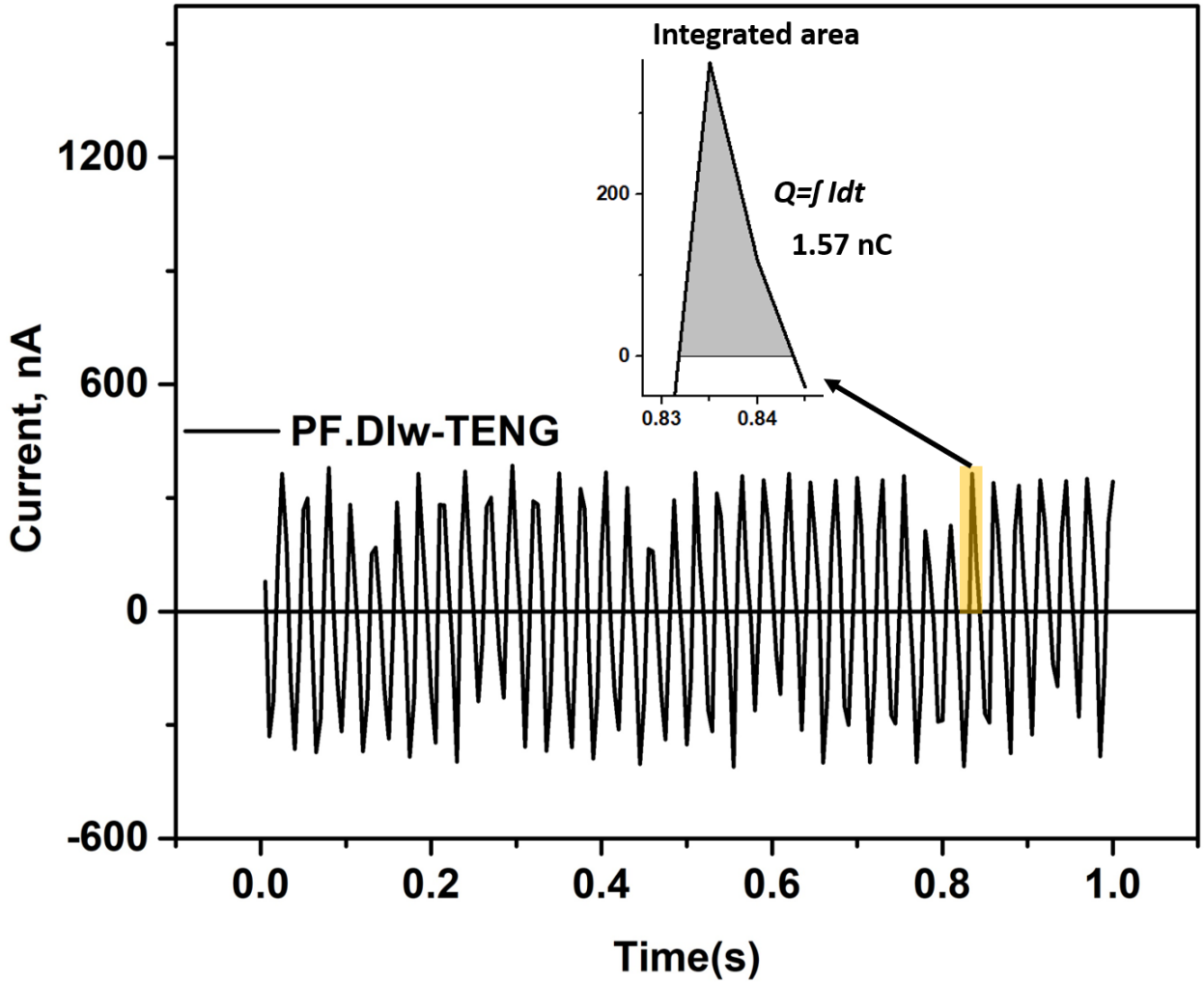

Fig. 4.11: Calculation of maximum induced colomb charge from the sampling time of 1s of the short circuit current for PF.DIw-TENG at 140 rpm. The transferred

charge is calculated by integrating the area between the single peak and the X-axis and the induced charge is 1.57 nC.

calculation for the induced colomb charge has shown in the fig. 4.11. The maximum induced Coulomb charges from a single peak from the 1s data are 2.31 nC, 2.89 nC, 4.72 nC, 6.56 nC for PF.Tw-TENG and 1.57 nC, 2.49 nC, 2.09 nC, 1.94 nC for the PF.DIw-TENG with the speed of 140, 210, 280 and 350 rpm as shown in inset images of fig. 6(a) and fig. 6(b) respectively. The corresponding maximum induced surface charge densities by a single peak of PF.Tw-TENG and PF.DIw-TENG were (2.45, 3.07, 5.01, 6.96) $\mu C/m^2$ and (1.67, 2.64, 2.22, 2.06) $\mu C/m^2$, respectively. The comparison of the charge densities for the both PF.TENGs have shown in the fig.4.12. From the graph, it is observed that, PF.DIw-TENG has shown decreasing trend with the increasing pump speed as DI water only contain the H^+ as positive ion and the interaction of very first moving H^+ ion is not enough with the mpPVDF membrane with the increasing values of the speed. According to charge conservation theory, charge can never be created nor destroyed. Therefore, the net amount of charge is always conserved in the universe; that is, a definite amount of positive charge is always neutralized by the same amount of negative charge. Therefore, with the mpPVDF membrane, the same amounts of opposite charges are induced in the fixed volume of tap water and DI water that is in contact with the membrane.

The current, voltage and Power output tests were performed to show the feasibility of the device for proper applications. The level of electric power depends on the load resistance in a system. Therefore, the PF-TENGs were connected to electrical resistors to apply an external load, and then the electric output was measured in order to evaluate the effective electric power of the PF-TENGs. With an increase of resistance, the instantaneous maximum voltage through the resistor generally increases and saturates upto the open-circuit voltage when the resistance is infinitely

large. The current across the resistor follows an opposite trend. The resistance range is from 0 to 25 MΩ, and the voltages increased from 4.5 V to 9V for PF.Tw-TENG, and from 3 V to 6V for PF.DIw-TENG. The currents decreased from 0.85 μA to 0.35μA for PF.Tw-TENG and 0.58 μA to 0.25 μA for PF.DIw-TENG, fig.4.10(c). The power output density was gradually increased and then decreased and then decreased, for instance, 8.43 mW/m^2 to 12.53 mW/m^2 for PF.Tw-TENG, and 6.7 mW/m^2 to 5.3 mW/m^2 for PF.DIw-TENG, respectively, with respect to the applied resistance of 0 to 25 MΩ, fig.4.10(d). The consistent peak voltage was found for the one hour operation of the both PF.TENGs as shown in fig. 4.10(e). The maximum output currents increment of PF.Tw-TENG in percentage with respect to PF.DIw-TENG are shown in fig. 4.10(f). At the maximum speed of 350 rpm, maximum 63.64% improvement has been observed for PF.Tw-TENG over PF.DIw-TENG.

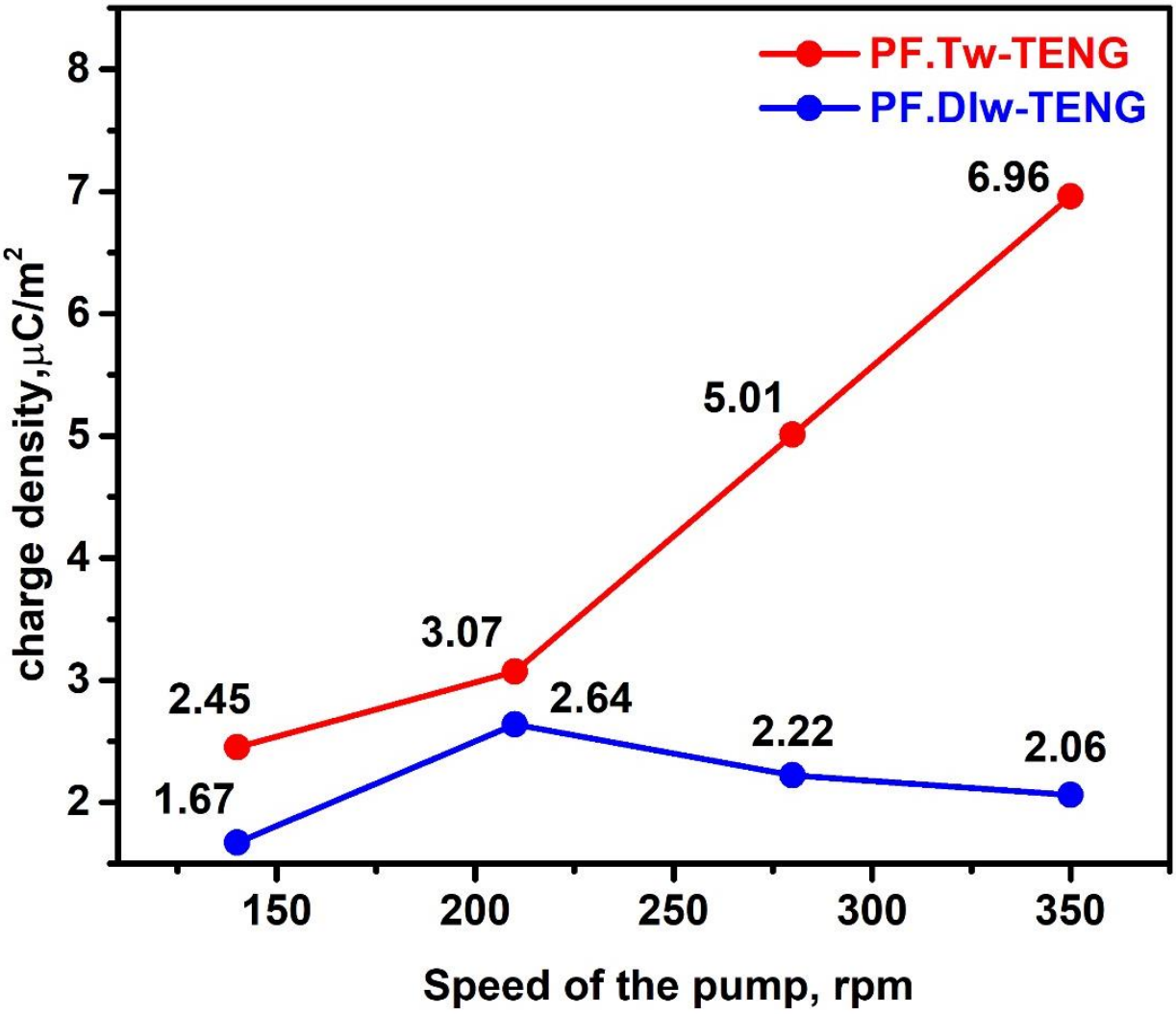

Fig. 4.12: Comparison of the induced maximum transferred charge density from a single peak for PF.Tw-TENG and PF.DIw-TENG at different pump speed.

4.7. Evaluation for stability and sensing

For the practical applications, the stability and durability of the PF-TENGs are very important for long term operation to acquire accurate values for sensing. For this purpose, the PF.Tw-TENG cell was kept for about one week in the open environment and again the experiment was performed, fig. 4.13(a). The performance is quite satisfactory but little bit low voltage output. This is not instability as overall outputs

are almost same over periodical measurement. The reason is still unclear, but it is to be believed that the uneven outputs are possibly caused by the surface morphological changes while interacting with the random ionic distribution of the flowing fluids. This can be easily solved by utilizing triboelectrically negative polymeric thin film that suited to the different characteristic of the working fluid. Fig.4.13(b) shows the rectified charging of a capacitor at three different speeds using the tap water. Fig. 4.13(c) shows the voltage peak for the average volumetric flow rates ranging (306ml/min- 766ml/min) of the tap water. With the increment of the flow rate, the voltage peaks also rise and fig. 4.13(d) shows the voltage peak linearly improves conformably. From this point of view, it can be said that, our simply fabricated PF-TENG can be easily used to detect the average volumetric flow rate of any small portion of transported ionic liquid used for various chemical industrial process or lab scale experiment. Moreover, it can be predicted that, the techniques can be used in biological process of blood stream supplied from the heart using biocompatible polymeric thin surface.

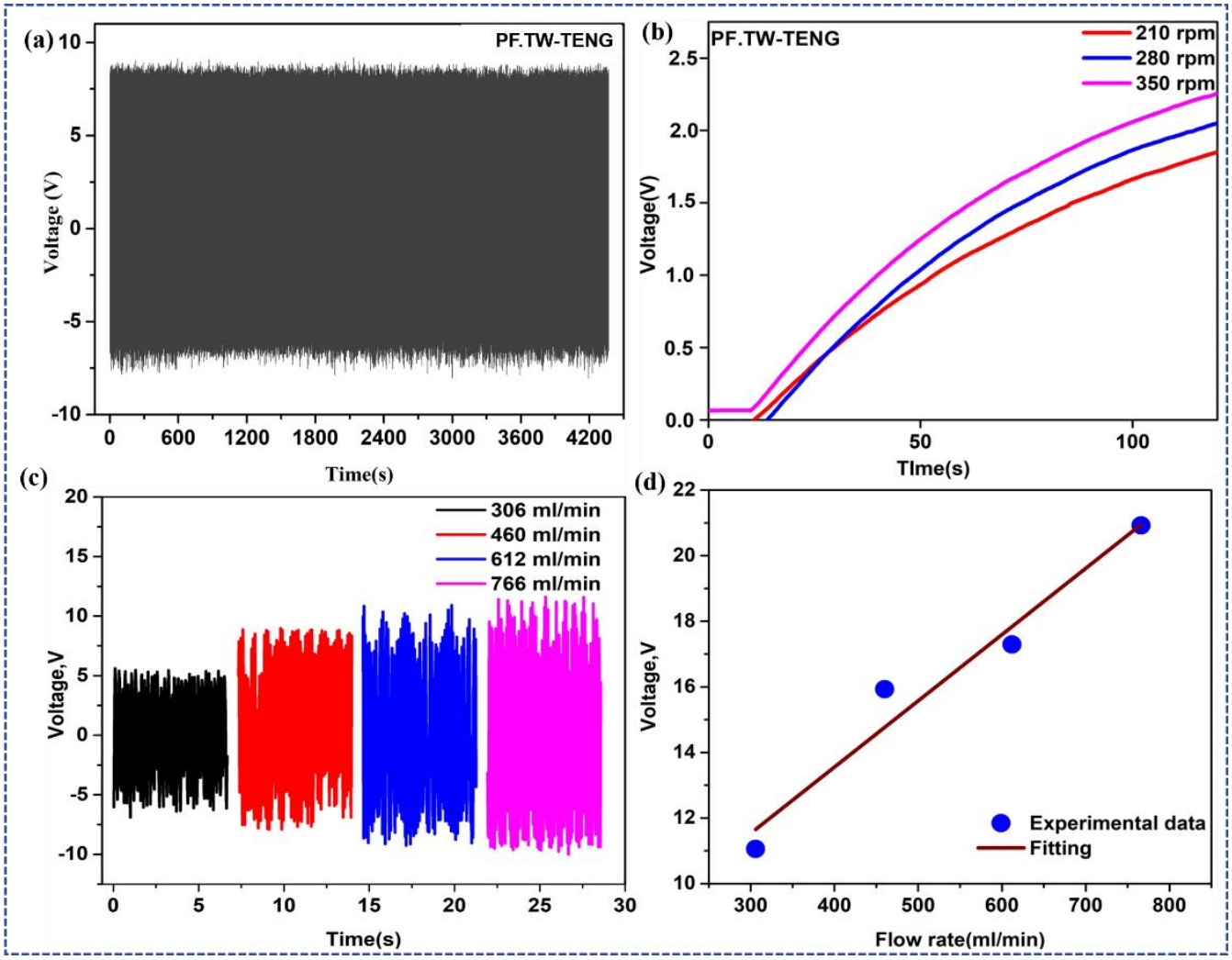

Figure 4.13. (a) Performance test after one week to check the realibility of PF.Tw-TENG; (b) Rectified output of the PF.Tw-TENG at different pump speed to charge a commercial capacitor of 4.7 μF; (c) Output voltage at varied average volumetric flow rate; (d) The linear relationship between voltage and average volumetric flow rate.

CHAPTER 5

DISCRETE LIQUID COLUMN BASED TENG USING MEMS

5.1. Analytical study of MEMS based TENG

MEMS based solid-liquid TENG has now become popular in microelectronics, diagnosis and chemical analysis. For MEMS based TENG, sensing capability has got importance rather than energy harvesting purpose. Electricity generation with flow in a micro channel has paved the way of micro/nano sensing for delicate measurement of pressure variation, angular displacement in precision engineering and mechanical motion. To achieve the best performance from micro, nano or mini channel based liquid TENG, hydrophobicity as well as slippery channel surface are considerable factors [61]. Slippery channel surface holds for Navier slip condition that allows the highly concentrated ions within the slip plane to be mobile [62,63]. From this perspective, surface irregularities or micro-roughness or chemical modification can be done to reduce the wetting behavior as well as increasing the air gap in the liquid-solid channel interaction. A lot of studies have done till now regarding channel flow and surface modification in fluid-based TENG. In 2016, Lee et. al. developed a microfluidic channel for pressure sensing and finger motion monitoring but didn't consider the fact of residual water that can stick to the channel surface. The output current was about 1.62nA at 11.6 N [64]. Choi et. al. investigated on self-powered ion concentration sensor for chemical detection of liquid. In his case, with DI water the current was generated up to 60 nA from ten microchannels [65]. Kim et. al. developed an air slug sensor by periodic injection of air and water in the two different PDMS channels with same cross-sectional area of 2 mm x 1.9 mm; lengths were 18 mm and 36 mm long respectively. In this experiment, 10 cm 0.01

M NaCl solution column was used to create the air gap. The peak to peak current was found 0.331 µA [66]. All the processes described above, though efficient but the fabrication process is expensive and time-consuming. So, an easily viable and inexpensive pathway is needed for the robust application and to replace the conventional sensory module.

In this chapter, a 3D printed micro-architectured PDMS (MA-PDMS) channel assisted liquid-solid TENG is proposed to measure the angular frequency with a certain amplitude and pressure fluctuation of the rotary actuator by deploying discrete DI water column inside the mini-channel and PTFE porous thin film as the counter solid material. The hydrophobicity of the channel surface satisfies Navier-stokes slip boundary condition and ensures stable output from the oscillation of the water column. The novelty of this free-standing mode TENG includes: (1) Cost-effective and simple approach for fabricating hydrophobic channel; (2) self-powered flexible and portable sensor to replace the conventional expensive measuring device in hydraulics and robotics manipulator, actuating device.

5.2. MEMS fabrication using PDMS polymer and 3D printed mold

To develop the mini-channel for DLC-TENG, instead of the conventional soft lithography process, we have adopted 3D printing technique to develop the micro structured pattern of the mini-channel on the prepared mold which is more viable and easier process.

5.3. Materials and methods

As the solid tribomaterial, porous PTFE thin film with 50 µm thickness was purchased from Good Fellow Material (GFM), Korea. PDMS sylgard-184 elastomer precursor part-A, precursor part-B were purchased from Dow Corning. Double distilled water (DI water) (Ultrapure system from our lab) was used for better

understanding the electrical output behavior of solid-liquid interaction phenomena in case of different test conditions. All the chemical substances and working liquids were used as received without any further purification process. To characterize the surface morphology and hydrophobicity FE-SEM was conducted by using a Hitachi cold FE-SEM microscopy which operates at 10 kV and contact angle of DI water was determined by the DSA 100 Goniometer (error 1^0) according to the sessile-drop method with 5 µL droplet (KRUSSG mbh, Hamburg, Germany).

5.3.1. Fabrication techniques of the MA-PDMS channel & DLC-TENG

As PDMS itself is hydrophobic in nature, so to improve the working function as well as hydrophobicity, micro/nano roughness is a considerable factor. The hierarchical surface roughness attributes to create the air gap between the water-solid

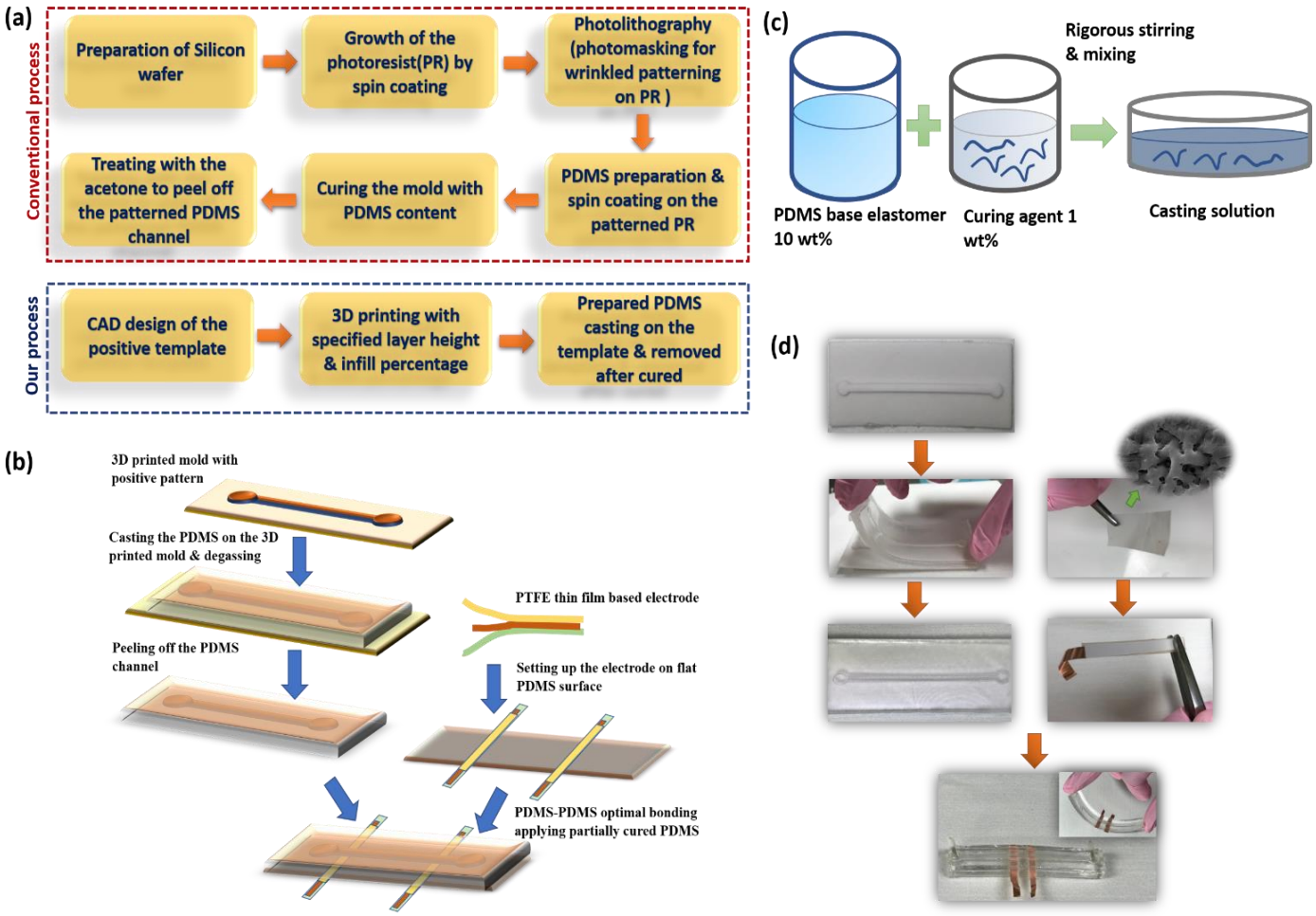

Fig.5.1. (a) Difference between conventional process and proposed process to develop the micro structured PDMS channel, (b) preparation of the PDMS casting solution from the base polymer and the curing agent, (c) Schematic diagram showing the fabrication of the PDMS channel, electrode setup on the flat PDMS and PDMS-PDMS bonding. (d) Experimental photograph of the fabrication techniques (Inset: FE-SEM image of the pristine porous PTFE thin film).

interface and water can easily slide over the surface if it is used as column or droplet and the phenomena have already reported by many literatures to develop the PDMS based channel [67,68]. Fig. 5.1 shows the schematic of the detailed procedure from

the fabrication of the micropatterned PDMS channel to the development of the DLC-TENG. Whereas the conventional process as depicted in Fig. 5.1(a) described in the above literatures to create microstructure based channel involves complicated fabrication process i.e. wafer cleaning and priming, sacrificial layer growth on the Si wafer, photolithography, pattern transfer, photoresist removal, wet etching, removal of the sacrificial layer by dipping into acetone, spin coating of the PDMS, curing and peeling off the patterned channel. on the contrary, our proposed method only consists of three easy steps to make the patterned channel which is very convenient and inexpensive method. A major advantage of this method is the precision of the pattern replication is improved, as any kind of surfactant coating is not required.

Fig. 5.1(b) shows the detailed procedure of the mini-channel preparation that utilizes the commercially available Fused deposition modeling 3D printing techniques to develop the desired template. The positive pattern of the channel was first designed with the inventor and then 3D printing technique was used to get the desired positive pattern as a casting template. The channel width and height were kept accordingly at 2.8 mm and 0.8mm. To create the micro surface roughness in the PDMS microchannel, we utilize the layer thickness and fill factor percentage of the FDM printer. The PLA (Poly Lactic Acid) material from our 3D printer Ultimaker Cura 3 was used in this process. At first, three kinds of template were prepared with the varying layer thicknesses (0.06, 0.15, 0.3 and 0.4) mm. Obviously, the 0.4 mm shows the better performance to generate the surface roughness on the PDMS. So, the layer thickness was set to 0.4 mm and the infill density was counted 50% for the linear infill pattern with the nozzle speed of 150 mm/s. The sample was developed by putting it on the XY plane in layer by layer formation process. The layer thickness can contribute to the generation of the roughness as reported by

Hartcher-O'Brien et.al. In the report, the roughness was varied in micro-meter level with the variation in the layer height [69]. For the 0.2 mm layer height, the roughness was found about 35 μm. After preparing the mold to cast the PDMS, at first the mold was rinsed with Iso-propyl alcohol, DI water and then dried in the hot plate for about half an hour. After that, PDMS precursor part-A and precursor part-B were mixed in 10:1 ratio and manually stirred for 10 minutes to get the uniformly mixed solution, Fig. 5.1(c). Then the solution was casted on the mold pattern and then degassed for one hour to remove excess air bubbles. After that, the casted PDMS with the mold was kept in the oven at 45^0C overnight. Then, the micro patterned PDMS channel with negative patterning was peeled off from the mold. While peeling off, no mold release material was used that has proved that the adopted procedure is very convenient, viable and reusable. Here, it is noted that, the temperature was kept low, as with the repeated experiment with high temperature it is found that, the polyacrylonitrile plastic shape can be deformed and can damage the proper shape of the PDMS channel. The micro-surface roughness has increased the hydrophobicity of the channel which has discussed in section 5.2.3.

To obtain the micro-surface roughness based flat PDMS, the same procedure was applied using flat 3D printed mold. PTFE thin film was cut into 2mm width strip and Cu foil tape was attached on the one side of the film. After that, the adhesive double-sided tape was attached on the bottom side of the Cu foil to complete the electrode making. The Cu foil width was kept nominal smaller than the PTFE film to make ensure the proper sealing to avoid the contact of the Cu foil with the liquid. After peeling off the cured flat PDMS the electrodes are attached on the rough surface.

To complete the fabrication of the DLC-TENG, partially cured PDMS-PDMS bonding technique has been done using PDMS mixture as adhesive [70]. Following this system, PDMS mixture with 10:1 ratio was applied on the patterned surface

other than the channel with the scrapping bar. The two-part was then procured at 40^0c for 30 minutes prior to bonding. After that, both parts gently pushed to each other such that no air bubble is existed and kept in the oven at 60^0 C overnight to get fully cured. Two holes with the same size were punched in the two ends and silicon tube was inserted into the hole to complete the fabrication of the DLC -TENG. Fig. 5.1(d) has represented the real photograph of the development of the proposed TENG.

5.4. Surface morphology characterization of the PDMS channel and porous PTFE thin film

Discrete liquid-solid contact electrification involves successive attachment and separation of liquid from the solid surface and therefore net electrical charge is generated. In this context, the solid surface from naturally inspired lotus leaf to triboelectrically sound laboratory developed fluoro-polymer or the polymer treated with silane, protein, etc. should exhibit the hydrophobic property that discrete volume of water can be rolled-off easily from the surface [71]. In our paper, the channel surface with micropatterned roughness facilitates the water column to flow spontaneously without leaving any residuals that satisfy the slip boundary condition $U \neq 0$; in case of mini-channel and effectively increase the uniform output of the electrical performance. Fig. 5.2(a) shows the FE-SEM images of the regularly patterned linear array of the micro convex curve produced by 3D printing in the inner surface of the PDMS channel which forms the micro air gap between the contact surface and the liquid. The contact angle, depicted in the inset image of the Fig. 5.2(a), was found 135^0 for the micro-architectured PDMS channel which proves the obvious hydrophobicity as well as a cost-effective technique to develop the hydrophobic surface. We also checked the FE-SEM and contact angle for the flat PDMS surface produced by 3D printed acrylic plastic material to distinguish the

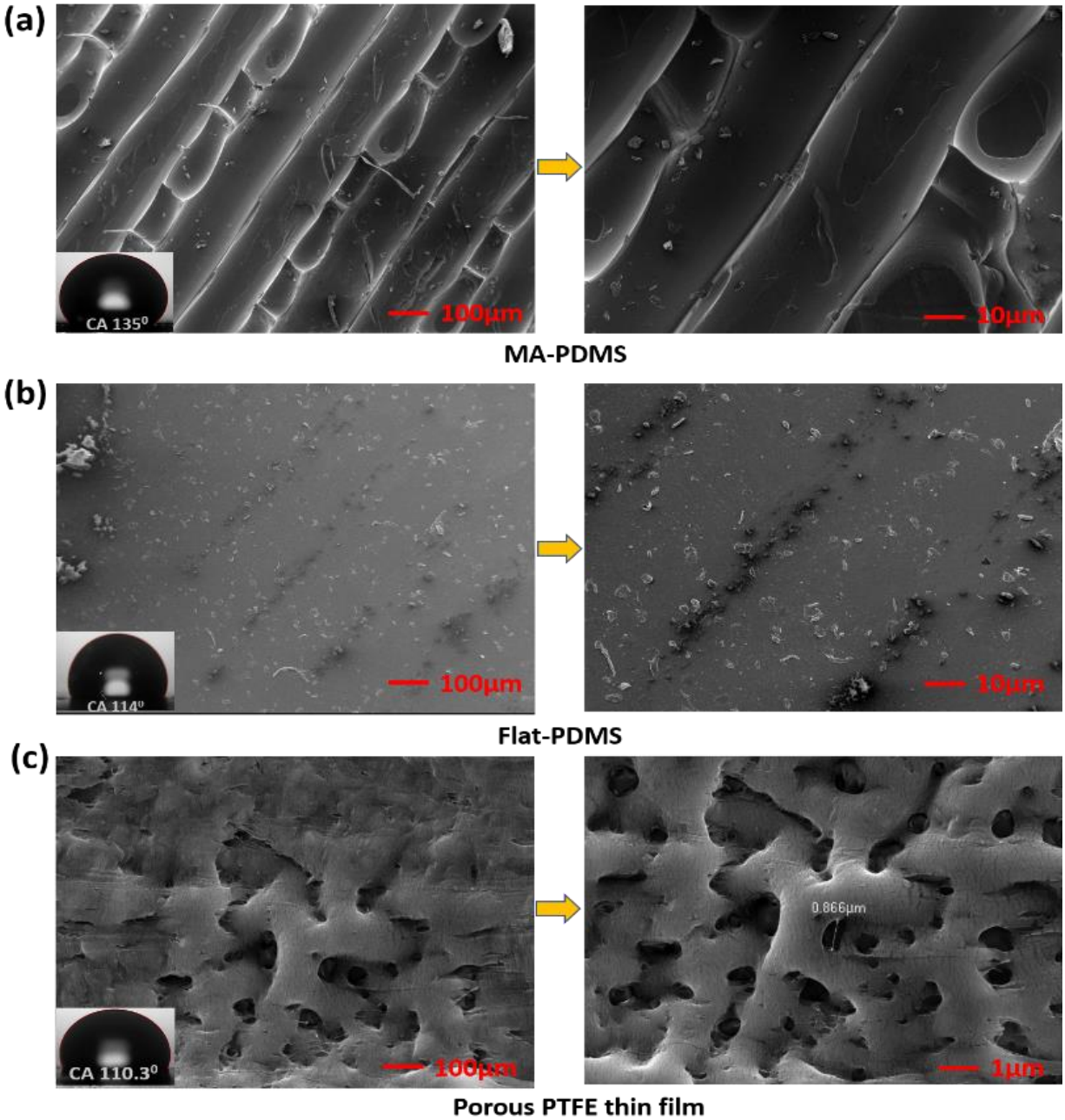

Fig. 5.2. FE-SEM images of (a) The micro-architectured PDMS inner surface; (b) The flat PDMS surface; (c) The porous PTFE thin film. (Inset images are the contact angle of each surface).

improved performance of MA-PDMS channel. In case of flat PDMS, the contact found was 114^0. For the development of the flat-PDMS, we have used the acrylic resin based transparent material in the stereolithography (SLA) printer from the central research facility of our university. In this process, the ultraviolet laser guide is passing back and forth according to the input model over the liquid plastic resin supplied from the resin tank and gradually cured it with the increasing temperature. After that, the model has dipped into the acetone to rub off the excess resin. The developed casting template is far smoother than the FDM produced template. Furthermore, the surface characteristics of the micro-porous PTFE thin film that comprises the DLC-TENG cell was analyzed and is shown in Fig.5.2(c). The micro-porosity with an average pore diameter of 0.866 µm of the commercially bought PTFE thin film produced the contact angle 110.3^0. The PTFE thin film has fluorine atoms at both end of long carbon chains which shows excellent water repellency and high electronegativity according to triboelectric series [72].

5.5. Working mechanism of the DLC-TENG

As shown in fig. 5.3(a), The DLC-TENG cell is comprised of flexible micropatterned PDMS channel with two microporous PTFE thin film-based electrodes attached inside the channel. The Cu adhesive tapes were shouldered with the copper wire to the capacitor to get the stable and regulated current and voltage signal. For measuring the electrical output of the DLC-TENG, a motion generator was used with controllable frequencies and amplitudes, incorporated by a rotary actuator (SMC-MSQ20A) that generated a pressure gradient for the water column sliding back and forth inside the channel. The actuator consists of a DC motor, adjustable arms connected with the motor shaft and can be synchronized with the frequency response and different amplitude of the pressure provided by the computer-controlled Arduino based IDE as shown in fig. 5.3(b). The inlet

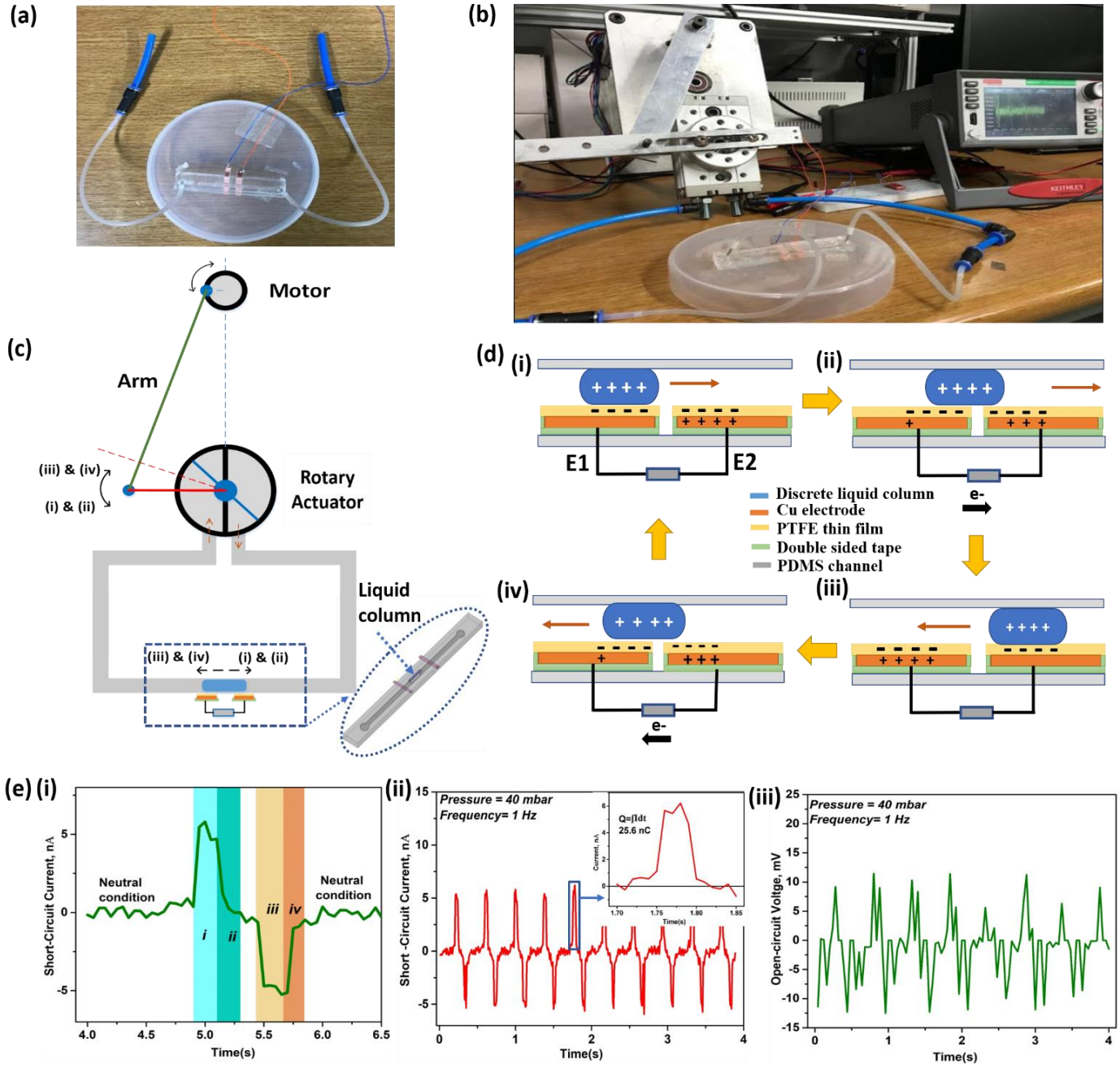

Fig.5.3. (a) Fabricated DLC-TENG cell with connecting silicon pipes. (b) Experimental setup of DLC-TENG with the rotary actuator. (Inset image of the Arduino IDE) (c) Schematic diagram to realize the oscillatory motion of DI water column with the angular rotation of the arm. (d) Mechanistic approach for generating V_{oc} and I_{sc} from the freestanding mode DLC-TENG. (e)(i) Magnified view of I_{sc}

showing the aforementioned four stages in (c) & (d) that contribute to the AC signal generation in one cycle rotation of the rotary actuator. At the pressure of 40 mbar and 1 Hz (ii) Open circuit voltage, (iii) Short circuit current.

compressed pressure was precisely controlled for different resonance frequency with fixed angular amplitudes ranging from 2.3 degrees to 5.6 degrees and different pressure values to get the desired precise electrical output from the oscillation of the water column inside the MA-PDMS channel.

The detailed working mechanism of the DLC-TENG is described in the Fig. 5.3(c) and Fig. 5.3(d) and the corresponding AC signal generation is illustrated in Fig. 5.3(e)(i) during repetitive motion of the liquid column in one cycle. The repetitive back and forth motion of the discrete DI water column over the two PTFE electrodes induces a triboelectric signal following freestanding sliding mode theory. At the steady state, the DI water column is positioned in the PDMS channel other than electrodes. As the PDMS is weakly negative according to the triboelectric series, it increases the positive charge on the surface of the water column by acquiring negative charge itself. When the arm of the rotary actuator moves in the anti-clockwise direction Fig.5.3(c), the water column moves over the surface of the PTFE thin film of electrode E(1), Fig.5.3(d). As the PTFE is highly triboelectrically negative, it induces maximum positive tribo-charges on the bottom surface of the water column. So, at the stage (i), the positive charges of the E1 electrode will be neutralized by the excess negative charges of the E2 electrode. When the water column starts approaching to E2 stated by the stage (ii) of Fig. 5.3(d), there is an electrostatic potential difference between E2 and E1 that drives the electron to move from E1 to E2.

During stage (iii), the water column fully covers the PTFE film of the E2 electrode so thus the Al electrode becomes fully neutralized by the excess release of

the electrons from the E1 electrode. After a while, the rotary arm starts to move in the clockwise direction as described in the Fig.5.3(c). So at the stage (iv) of Fig.5.3(d), the water column tends to approach towards the E1 electrode causing electrostatic imbalance again and increasing potential is diminished by the electron flow from the E2 to E1. Thus, the water column reaches at the stage (i) causing the repetition of another cycle. Fig. 5.3(e)(i) shows the consecutive positive-negative peak of short circuit current of a single oscillation of liquid column that is compatible with the charge generation behavior during the clockwise and anti-clockwise movement of the rotary actuator. During the anticlockwise direction, positive peak comes out with respect to the E1 electrode and continuously peak is decreasing with the water column leaving the electrode, the negative peak with the clockwise direction of the actuator denotes the water column is situated over the E2 electrode and continuously reaching the equilibrium state after completely covering the E1 electrode. The phenomenon indicates that the measured output data are in line with the agreement of the predicted theoretical AC behavior as reported in the previous kinds of literature.

5.6. Application as self-powered sensor

5.6.1. Pressure and frequency sensing of rotary actuator

The quantitative performance of the DLC-TENG was evaluated to show the effective performance of this simply fabricated device for active sensing of pressure fluctuation and frequency of the rotary oscillator. For this, 2.5 ml of DI water was injected in the channel to generate the oscillation motion in the channel. Fig. 5.3(e)(ii) and Fig. 5.3(e)(iii) show the short circuit current and open circuit voltage at the pressure of 40 mbar and frequency of 1 Hz. The DLC-TENG generates peak to peak open-circuit voltage and short circuit current up to 11.82 nA and 23.2 mV respectively without the additional power supply. Furthermore, under different

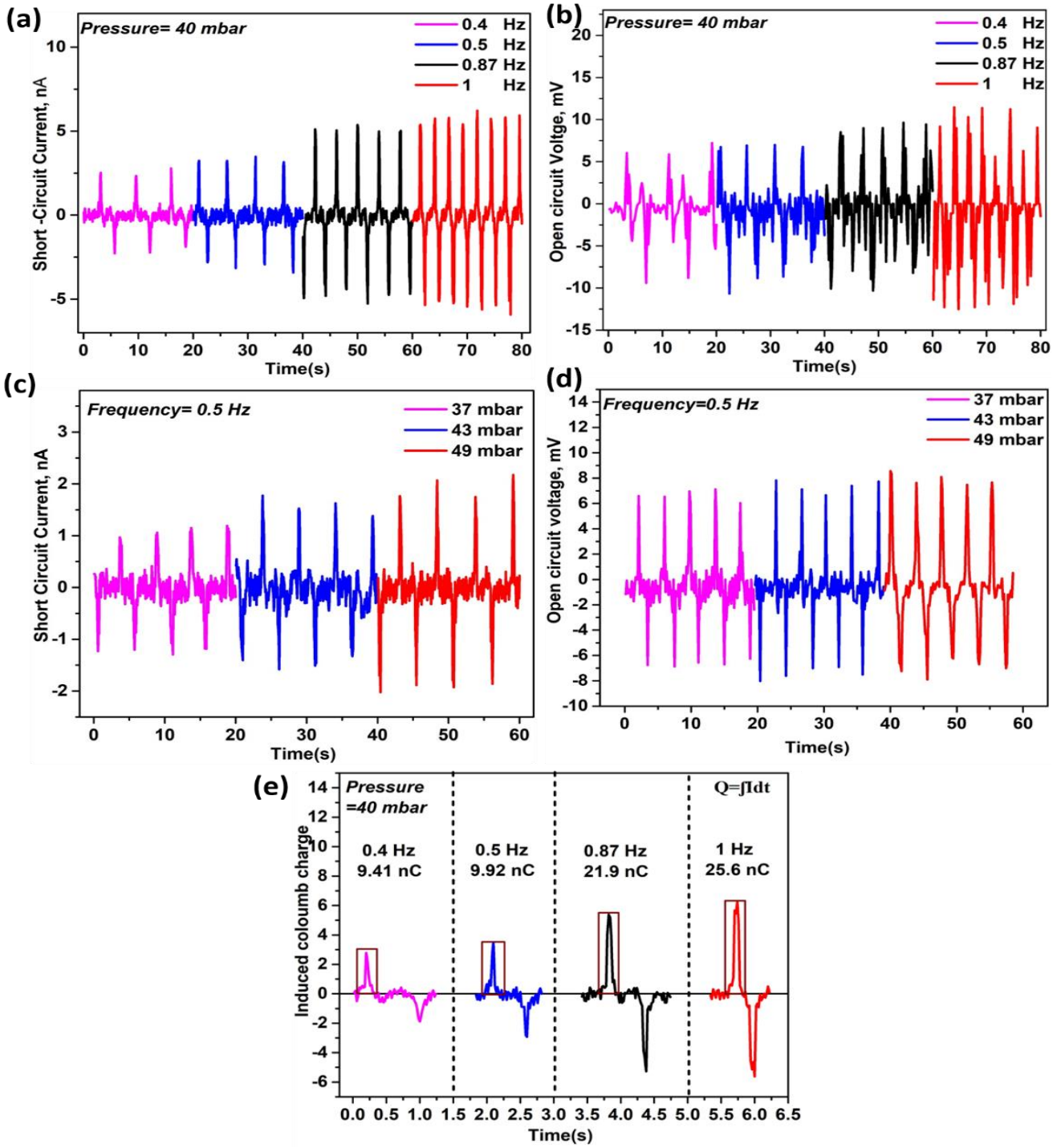

Fig 5.4. Short circuit current and open circuit voltage at different oscillation frequency of the (a) & (b), at different pressure gradient (c) & (d), respectively. (e) Induced coulomb charge for different frequency at the pressure of 40 mbar.

frequency cycle of specific pressure gradient, both the open circuit voltage and short circuit current show considerably concurrent signal over sequential measurements. The output performance of the DLC-TENG was characterized by the behavior of the current and voltage output under difference frequency cycle of the rotary oscillator maintaining fixed pressure with definite amplitude and variable pressure gradients. In case of frequency response behavior of the AC signal output, the pressure profile was maintained like triangular amplitude to observe that the proposed DLC-TENG is instantaneously responsive to the sudden fluctuation of pressure. As shown in Fig. 5.4(a) and Fig.5.4(b), with the fixed pressure value of 40 mbar, the frequencies of the back and forth motion of the rotary oscillator were kept 0.4 Hz, 0.5 Hz, 0.87 Hz and 1 Hz. Under these resonance frequencies, the peak to peak short circuit current and open circuit voltage of the oscillating water column are 4.43 nA, 6.41 nA, 10.5 nA, 11.82 nA; 11.8 mV, 15.6 mV, 19.2 mV, 23.9 mV, respectively. From this observation, the uniform AC signal shows good performance with the increment of the frequency. For different pressure values applied with a frequency of 0.5 Hz, the output data was analyzed as depicted in Fig. 5.4(c) and 5.4(d). The I_{sc} and V_{oc} (Peak to peak) for 37, 43 and 49 mbar are 2.33 nA; 3.27 nA; 3.97 nA, 13.56 mV; 15.42 mV; 15.58 mV, respectively. Though the voltage output was slightly varied when the pressure value changes from 43 and 49 mbar but the current values can be distinguished to be effectively utilized as a pressure sensor. The induced coulomb charges with 0.4, 0.5, 0.87 and 1 Hz are 9.41 nC; 9.92 nC; 21.9 nC; 25.6 nC, respectively and is shown in fig. 5.4(e). It is to be noted that, the peak to peak I_{sc} and V_{oc} for each frequency and pressure value were analyzed over a definite time interval. As to quantify a triboelectric nanogenerator for the self-powered sensor, time is an

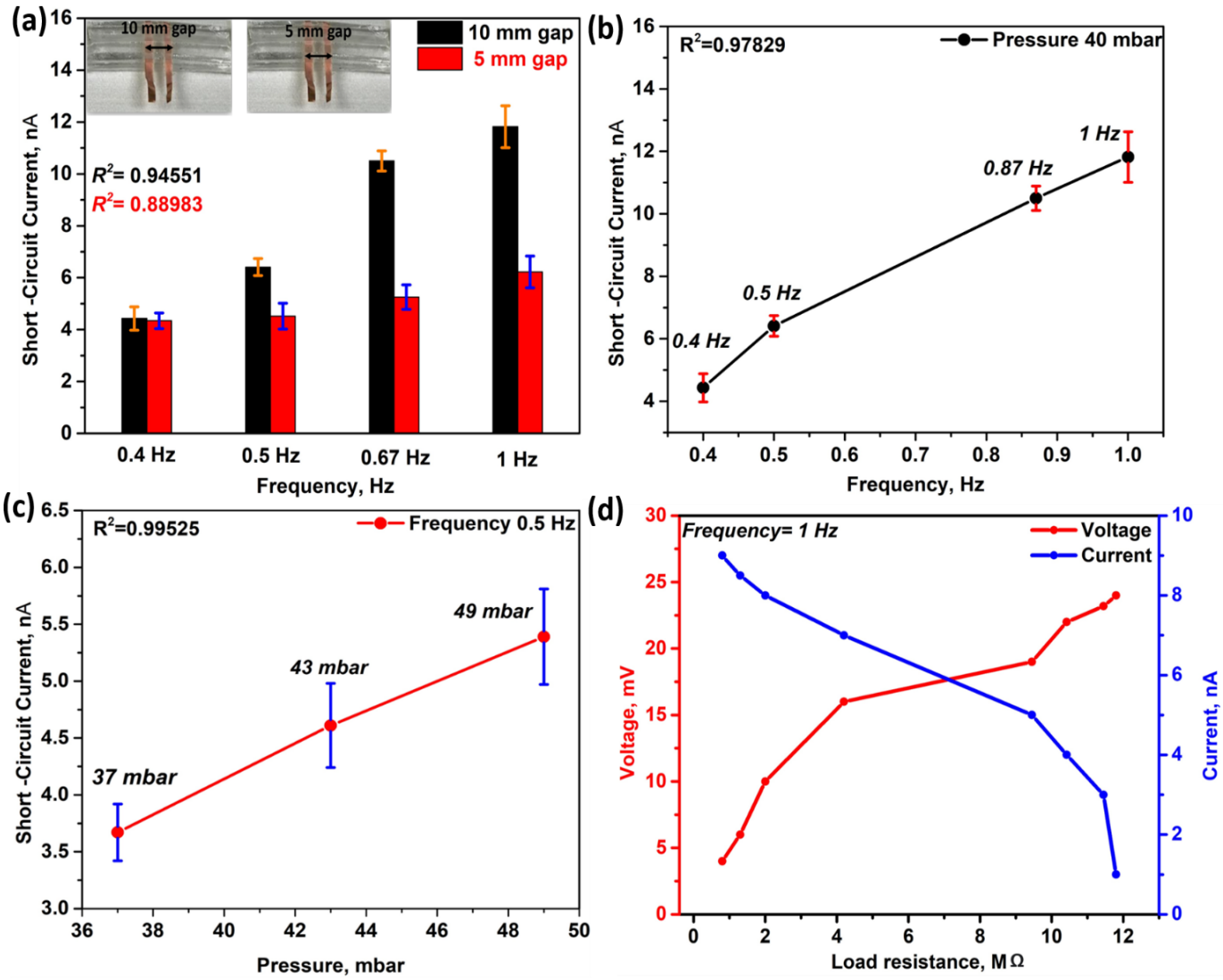

Fig. 5.5. (a) Short circuit current at the various frequency for 10 mm and 5 mm electrode gap. The linear increasing trend of the current curve with respect to the (b) frequency and (c) pressure variation response to be applied as a sensor. (d) At the frequency of the 1 Hz the voltage and current output against different load resistance.

essential factor. The generated I_{sc} and V_{oc} should be stable over a certain time period at the same parameter, otherwise the proposed system can't be regarded as a sensor. The DLC-TENG performance was visualized by employing one PDMS channel in the experimental setup but varying the gap of the electrode. Fig. 5.5(a) shows the I_{sc}

of the 5 mm and 10 mm of a gap of the electrode while the discrete liquid column volume and position was kept fixed. For all frequencies, the DLC-TENG cell, with the 10 mm electrode gap between them shows better performance. As it can be explained that, with the reduction of the gap of the electrode, the water column moves back and forth very fast over the polymer surface, hence the water column doesn't have enough time interval for the charge to be induced consequently generates lower output. The prospect of the DLC-TENG as a frequency and pressure measurement device is illustrated in fig. 5.5(b) & fig. 5.5(c) respectively. The tendency of the curves is almost linear with frequency and pressure responses. Finally, to be realized as a self-powered device, the voltage and current were measured with respect to different load resistance at the frequency of 1 Hz as shown in fig. 5.5(d). The resistance was varied from the 0 to 12 MΩ and the maximum voltage of 25 mV and current of 9 nA were found at 12 MΩ and 1 MΩ respectively. From this observation, it is conspicuous that our proposed DLC-TENG can be effectively applied for the self-powered robust, flexible, cost-effective, easily fabricated transducer, where observing small scale change of physical properties is needed to be observed.

Chapter 6

Conclusions

(1) In a nutshell, In chapter 4, we have demonstrated an elastic tubing based TENG that can grab energy from the unsteady pulsatile flow of the DI water, tap water. The fabrication of the mpPVDF membrane inside the flexible silicone pipe is easy, commercially viable, eco-friendly, and portable. The proposed PF-TENG is highly durable and can be used with lower volumes of feed-stocks to generate desirable amount of voltage and I_{sc}. The mechanistic approach based on the EDL formation and pulsatile movement of the liquid that relates the hydrodynamics with the surface electric potential of the polymeric membrane has supported the generation of voltage and currents in our PF-TENG system. The PF.DIw-TENG, PF.Tw-TENG showed a output voltage and I_{sc} of 10 V and 0.46 µA, 20.92 V, 0.95 µA at 350 rpm, respectively. The PF. Tw-TENG also showed stable performance after one-hour durability test. The output power density has increased by 3.6 times in case of tap water over DI water due to the availability of more ions in the EDL, which enhanced the conductivity of the tap water. This experiment has shown that this cell can be used as self-powered flow rate measuring system that is cost effective and is of important in peristaltic transportation of the liquid products.

(2) In summary, in chapter 5, a regular AC output has obtained from the DLC-TENG to be effectively utilized for sensing applications and energy harvesting. The developed DLC-TENG with easy fabrication techniques is eco-friendly and portable. The proposed TENG is highly durable with lower volumes of injected liquid in the channel to generate the desirable consistent output of V_{oc} and I_{sc}. The mechanistic pathway evolved in the system based on free-standing sliding mode TENG from the cited previous reports has supported the generation of current and voltage. The

surface morphology, checked by the FE-SEM, has proved the obvious structural change of the contact surface and further improved hydrophobicity has confirmed by the contact angle analysis. The DLC-TENG has shown sensible response to the different frequency and pressure values. Therefore, we expect that our self powered DLC-TENG would provide a simple way for possible application in various physical parameter sensing and detection.

ACKNOWLEDGEMENT

This research was supported by Basic Science Research Program through the National Research Foundation of Korea (NRF) funded by the Ministry of Science and ICT, South Korea (NRF-2017R1A2B3004625).

PUBLICATIONS

1. ***"Harvesting liquid stream energy from unsteady peristaltic flow induced pulsatile flow-TENG (PF-TENG) using slipping polymeric surface inside elastomeric tubing"***, Ravi Kumar Cheedarala[1], **M. Shahriar[1]**, Jee Hwan Ahn, Jeong Yun Hwang, Kyoung Kwan Ahn, ***Nano Energy,*** Vol. 65, 104017, 2019**.** https://doi.org/10.1016/j.nanoen.2019.104017 **(Co-first author). Elsevier.**

2. ***"Self-Powered Flexible PDMS Channel Assisted Discrete Liquid Column Motion Based Triboelectric nanogenerator (DLC-TENG) as Mechanical Transducer"*, M. Shahriar,** Cong Phat Vo, Kyoung Kwan Ahn, ***Int. J. of Precis. Eng. and Manuf. - Green Tech*.** https://doi.org/10.1007/s40684-019-00148-8 **Springer Nature.**

REFERENCES

1. Wang, Z.L., Zhu, G., Yang, Y., Wang, S.H., Pan, C.F.," Progress in nanogenerators for portable electronics" Mater. Today, Vol.15, No. 12, pp.532-543, 2012.

2. X. Wang, "Piezoelectric nanogenerators-Harvesting ambient mechanical energy at the nanometer scale", Nano Energy, vol.1, pp.13-24, 2012.

3. Y. Hu, Z.L. Wang, "Recent progress in piezoelectric nanogenerators as a sustainable power source in self-powered systems and active sensors", Nano Energy, 2015, 14,3

4. Y. Yang, W. Guo, K.C. Pradel, G. Zhu, Y. Zhou, Y. Zhang, Y. Hu, L. Lin, Z. L. Wang, "Pyroelectric Nanogenerators for Harvesting Thermoelectric Energy, Nano Lett., 12, 2833, 2012.

5. W. Tang, B. D. Chen, Z.L. Wang, Recent Progress in Power Generation from Water/Liquid Droplet Interaction with Solid Surfaces, Adv. Funct. Mater. 2019, 1901069, p.1-13.

6. Z. L. Wang, Triboelectric Nanogenerators as New Energy Technology and Self-Powered Sensors-Principles, Problems and Perspectives. Faraday Discussions, Vol. 176, 2014, 447-458.

7. S. Wang, L. Lin, Z.L. Wang, "Triboelectric Nanogenerators as self-Powered active sensors", 11(2015), 436-432.

8. Z. H. Lin, G. Cheng, S. Lee, K.C. Pradel, Z.L. Wang, "Harvesting Water Drop Energy by a Sequential Contact-Electrification and Electrostatic Induction Process", Adv. Mater., 26(2014) 4690-4696.

9. S. Niu, Y. Liu, S. Wang, L. Lin, Y. S. Zhou, Y. Hu, Z.L. Wang, "Theoretical

Investigation and structural Optimization of Single-electrode Triboelectric nanogenerators", Adv. Mater. 27(2015), 1316-1326.

10. Z.L. Wang, L. Lin, J. Chen, S. Niu, Y. Zi, "Triboelectric Nanogenerators", Springer, Berlin, 2016.

11. B. Zhang, L. Zhang, W. Deng, L. Jin, F. Chun, H. Pan, B. Gu, H. Zhang, Z. Lv, W. Yang, Z. L. Wang, "Self-Powered Acceleration Sensor based on Liquid Metal Triboelectric Nanogenerator for Vibration Monitoring," ACS Nano 11(2017), 7440-7446.

12. S. Niu, Y. liu, X. Chen, S. Wang, Y. S. Zhou, L. Lin, Y. Xie, Z. L. Wang, "Theory of Freestanding Triboelectric Layer based Nanogenerators", Nano Energy, 12(2015), 760-774.

13. J. Bae, J. Lee, S. Kim, J. Ha, B.S. Lee, Y. Park, C. Choong, J.B. Kim, Z.L. Wang, H.Y. Kim, J.J. Park, U.I. Chung, "Flutter-driven triboelectrification for harvesting wind energy", Nat. Commun., 5, p. 4929, 2014.

14. Lee, E.K., Yin, L., Lee, Y., Lee, J.W., Lee, S.J., Lee, J., Cha, S.N., Whang, D., Hwang, G.S., Hippalgaonkar, K., Majumder, A.,Yu, C., Choi, B.L., Kim, J.M., Kim, K.,"Large Thermoelectric Figure-of-merits from SiGe Nanowire by Simultaneously Measuring Electrical and Thermal Transport Properties," Nano Letters, Vol.12, pp. 2918, 2012.

15.Lee, J.H., Lee, Y.K., Gupta, M.K., Kim, T.Y., Lee, D.Y., Oh, J., Ryu, C., Yoo, W.J., Kang, C.Y., Yoon, S.J., Yoo, J.B., Kim, S.W., "Highly Stretchable Piezoelectric-Pyroelectric Hybrid Nanogenerator" Advanced Materials, Vol. 26, pp. 765, 2014.

16.Yang, Y., Jung, J.H., Yun, B.K., Zhang, F., Pradel, K.C., et.al., “Flexible Pyroelectric Nanogenerators Using a Composite Structure of Lead-Free KNbO3 Nanowires,” Advanced Materials, Vol. 24, No. 39, pp. 5357-5362, 2012.

17. Beeby, S. P. “A micro electromagnetic generator for vibration energy harvesting.” J. Micromech. Microeng. Vol. 1, 1257-1265, 2007.

18. Mehmet Kanik, Nanostructured materials and devices for sensing and energy harvesting applications, PhD thesis, 2015.

19. W. Tang, T. Jiang, F. R. Fan, A. F. Yu, C. Zhang, X. Cao, Z. L. Wang “ Liquid-metal electrode for high-performance triboelectric nanogenerator at an instantaneous energy conversion efficiency of 70.6%” Adv. Funct. Materials, 3718-3725, 2015.

20. X. Zhang, Y. Zheng, D. Wang, F. Zhou, “Solid-liquid triboelectrification in smart U-tube for multifunctional sensors”, Nano Energy, 95-106, 2017.

21. Z. H. Lin, G. Cheng, S. Lee, K. C. Pradel, Z. L. Wang, “Harvesting water drop energy by a sequential contact-electrification and electrostatic induction process”, Adv. Mat., 1-7, 2014.

22. M. Xu, S. Wang, S.L. Zhang, W. Ding, P. T. Kien, C. Wang, Z. Li, X. Pan, Z. L. Wang, “A highly sensitive wave sensor based on liquid-solid interfacing triboelectric nanogenerator for smart marine equipment”, Vol. 57, pp. 574-580, 2019.

23. T. Jiang, L. M. Zhang, X. Chen, C. B. Han, W. Tang, C. Zhang, L. Xu, Z.L. Wang, “Structural Optimization of Triboelectric Nanogenerator for Harvesting Water Wave Energy,” ACS Nano 9(2015) 12562-12572.

24. L. Xu, Y. Pang, C. Zhang, T. Jiang, X. Chen, J. Luo, W. Tang, X. Cao, Z. L. Wang, “Integrated Triboelectric Nanogenerator Array Based on Air-driven

Membrane Structures for Water Wave Energy Harvesting," Nano Energy, 31(2017), p. 351-358.

31. Choi, Y.W., Jang, S., Chun, M.S., Kim, S.M., Choi, M., "Efficient microfluidic power generator based on the interaction between DI water and hydrophobic channel surface," Vol. 15, No. 2, pp. 255-260.

32. Y. He, J. Lao, T. Yang, X. Li, X. Zang, X. Li, M. Zhu, Q. Chen, M. Zhong, H. Zhu, Galvanism of continuous ionic liquid flow over graphene grids, Appl. Phys. Lett. 107, 081605(2015).

33. J. Yin, X. M. Li, J. Yu, Z. H. Zhang, J.X. Zhou, W.L. Guo, Nature Nanotechnology, Vol. 9, pp.378, 2014.

34. Y. Xu, P. Chen, J. Zhang, S. Xie, F. Wan, J. Deng, X. Cheng, Y. Hu, M. Liao, B. Wang, X. Sun, H. Peng, A One-Dimensional Fluidic Nanogenerator with a High Power Conversion Efficiency, Angew. Chem. Int. Ed. Vol. 56, pp. 12940-12945, 2017,

35. S. Srinivas, S, Sreenadh, C.K. Selvi, Peristaltic pumping of a Generalized Newtonian Fluid in an Elastic Tube, Journal of App. Fluid Mechanics, Vol.10, No.6, 1785-1798, 2017.

36. Takagi, D. And N. J. Balmforth, Peristaltic pumping of viscous fluid in an elastic tube, J. Fluid Mech. 672, pp.196-218, 2011.

37. Misery, A. M. E., Elsayed F. Elshehawey and A. A.Hakeem, Peristaltic motion of an incompressible generalized Newtonian fluid in a planar channel. Journal of physical Society of Japan 65, pp.3524-3529, 1996.

38. Abd El, H., A. E. M. El Misery and I. E. Shamy, Hydrodynamic flow of generalized Newtonian fluid through a uniform tube with peristalsis. Appl. Math. Comp. 173, 856-871, 2006.

39. Pandey, S. K. and M. K. Chaube, Peristaltic transport of a visco-elastic fluid in a tube of a non-uniform cross section. Mathematical and Computer Modelling. Vol.52, pp. 501-514, 2010.

40. T. W. Latham, Fluid motions in a peristaltic pump. MS thesis, Massachusetts Institute of Technology, Cambridge, 1996.

41. Burns, J.C., and T. Parkes. Peristaltic motion. J. Fluid Mech.Vol.29, pp.731-743, 1967.

42. Fung, Y.C. and C.S. Yih. Peristaltic transport. J. Appl. Mech. Trans ASME. Vol.5, pp.669-675, 1968.

43. J. Manner, A. Wessel, T. M. Yelbuz, How does the Tubular Embryonic Heart Work? Looking for the Physical Mechanism Generating Unidirectional Blood Flow in the Valveless Embryonic Heart Tube, Dev. Dyn., Vol.239, pp. 1035-1046, 2010.

44. F. Boselli, J. B. Freund, J. Vermot, Blood Flow mechanics in Cardiovascular development, Cell Mol Life Sci. 72(13), 2015, 2545-2559.

45. A.V., Mernone, A mathematical study of peristaltic transport of a casson fluid, Math. and com. Modelling, 200204.

46. J. Yang, D., Y., Kwok, Microfluidic Flow in Circular Microchannel with Electrokinetic Effect and Naviers Slip Condition, Langmuir, Vol.19, No.4, pp.1047-1053, 2003.

47. Y. Ren, D. Stein, Slip Enhanced Electrokinetic Energy Conversion in Nanofluidic Channels, nanotechnology, Vol. 19, No.19, Paper no. 195707, 2008.

48. www.k-water.or.Kr

49. C. Hughes, L.-H. Yeh, S. Qian, J. Phys. Chem. C 117, 9322-9331, 2013.

50. P. Joseph, P. Tabeling, Direct Measurement of the apparent Slip Length, Physical Review E, Vol. 71., No. 3, Paper No. 035303, 2005.

51. L. Joly, C. Ybert, E. Trizac, L. Bocquet, Hydrodynamics within the Electrical Double Layer on Slipping Surfaces,

52. www.comsol.com

53. N. Elabbasi, J. Bergstrom, S. Brown, Fluid-Structure Interaction Analysis of a Peristaltic Pump, Proc. Of the 2011 COMSOl Conference, Boston, USA.

54. G.H. Bolt, Analysis of the validity of the Guoy-Chapman theory of the electric double layer, J.Colloid Sci. 10, 206-218, 1955.

55. M. Lungu, Electrical separation of Plastic materials using the triboelectric Effect, Min. Eng. 17, 69-75, 2004.

56. F.M. White, Fluid Mechanics, third ed. McGraw-Hill, 1994.

57. B. Fan, A. Bhattacharya, P.R. Bandaru, Enhanced Voltage Generation through Electrolyte Flow on Liquid-filled Surfaces. Vol.9, 4050, 2018.

58. Park, H., Choa, S.H., "Measurement of liquid flow rate by self-generated electrokinetic potential on the microchannel surface of a solid," Sensors and Actuators A: Physical, Vol. 208, pp.88-94, 2014.

59. J.M. Berg, T. Dallas, Peristaltic Pumps, Encyclopedia of Microfluidics and Nanofluidics, 2013.

60. https://motion.schneider-electric.com/success-stories/peristaltic-pumps/

61.Yang, J., Kwok, D. Y., "Microfluid Flow in Circular Microchannel with Electokinetic Effect and Navier's slip Condition," Langmuir, Vol. 19, No.4, pp.1047-1053, 2003.

62.Ren, Y., Stein, D., "Slip-Enhanced Electrokinetic Energy Conversion in Nanofluidic Channels," Nanotechnology, Vol. 19, No.19, paper no. 195707, 2008.

63.Choi, Y.W., Jang, S., Chun, M. S., Kim, S. M., Choi, M., “Efficient Microfluidic Power Generator Based on Interaction between DI Water and Hydrophobic-channel Surface”, International Journal of Precision Engineering and Manufacturing-Green Technology, Vol.5, Issue 2, pp. 255-260, 2018.

64.Shi, Q., Wang, H., Wang, T., lee, C.,” Self-Powered Liquid Triboelectric Microfluidic Sensor for Pressure Sensing and Finger Motion Monitoring applications,” Nano Energy, Vol.30, pp. 450-459, 2016.

65.Jeon, S.-B., Seol, M-K., Kim, D., Park, S.J., Choi, Y-K., ”Self-Powerd Ion Concentration Sensor with Triboelectricity from Liquid-solid Contact Electrification,” Vol.2, Article no. 1600006, 2016.

66.Y. Yang, J. Park, S. Kwon, Y.S. Kim,”Fluidic Active Transducer for Electricity Generation”, Sci.Rep., Vol.5, Art. No. 15695, 2015.

67.A. Tropmann, L. Tanguy, P. koltay, R. Zengerle, L. Riegger, “Completely superhydrophobic PDMS Surfaces for Microfluidics”, Langmuir, Vol. 28, No.22, pp. 8292-8295, 2012.

68.C.Feng, G. Zisheng, L. Dongxu,” Preparation of Material Surface Structure Similar to Hydrophobic Structure of Lotus Leaf”, J. of Wuhan University of Tech.-Mater Sci. Ed., Vol. 23, No.4, PP. 513-517, 2007.

69. J. Hartcher-O’Brien, J. Evers, E. Tempelman, “Surface Roughnress of 3D Printed Materials: Comparing Physical Measurements and Human Perception. ” Mater. Today Comm., Vol.19, pp. 300-305, 2019.

70.Eddings, A. M., Johnson, A. M., Gale, K.B., “Determining the Optimal PDMS-PDMS Bonding Technique for Microfluidics Devices,” Journal of Micromechanics and Microengineering, Vol. 18, Article no. 067001, 2008.

71.Choi, D., Kim, D.W., Yoo, D., Cha, J. K., La, M., Kim, S. D., “Spontaneous

occurrence of Liquid-Solid Contact Electrification in Nature: Toward a robust Triboelectric Nanogenerator Inspired by the Natural Lotus Leaf," Nano Energy, Vol. 36, pp. 250-259, 2017.

72.www.alphalabinc.com/triboelectric-series/